creative commons

COMMONS DEED

저작자표시-비영리-변경금지 2.0 대한민국

이용자는 아래의 조건을 따르는 경우에 한하여 자유롭게

- 이 저작물을 복제, 배포, 전송, 전시, 공연 및 방송할 수 있습니다.

다음과 같은 조건을 따라야 합니다:

저작자표시. 귀하는 원저작자를 표시하여야 합니다.

비영리. 귀하는 이 저작물을 영리 목적으로 이용할 수 없습니다.

변경금지. 귀하는 이 저작물을 개작, 변형 또는 가공할 수 없습니다.

- 귀하는, 이 저작물의 재이용이나 배포의 경우, 이 저작물에 적용된 이용허락조건을 명확하게 나타내어야 합니다.
- 저작권자로부터 별도의 허가를 받으면 이러한 조건들은 적용되지 않습니다.

저작권법에 따른 이용자의 권리는 위의 내용에 의하여 영향을 받지 않습니다.

이것은 이용허락규약(Legal Code)을 이해하기 쉽게 요약한 것입니다.

Disclaimer

dCollection

Ph.D. Dissertation of Natural Sciences

The Place Code in the Hippocampal Subregions CA1 and CA3 upon Visual Change in the Environment

해마 하위 영역 CA1과 CA3의 시각 자극 변화에 따른 장소 표상 패턴 연구

February 2023

Graduate School of Natural Sciences
Seoul National University
Brain and Cognitive Science Major

Jhoseph Shin

The Place Code in the Hippocampal Subregions CA1 and CA3 upon Visual Change in the Environment

Inah Lee

Submitting a Ph.D. Dissertation of
Natural Sciences

December 2022

Graduate School of Natural Sciences
Seoul National University
Brain and Cognitive Science Major

Jhoseph Shin

Confirming the Ph.D. Dissertation written by
Jhoseph Shin

December 2022

Chair	이석호	(Seal)
Vice Chair	이인아	(Seal)
Examiner	LEE SANG AH	(Seal)
Examiner	김형구	(Seal)
Examiner	곽지현	(Seal)

Abstract

Any events or experiences in the given space and time are stitched together as an episode. The hippocampus has been widely acknowledged for its role in episodic memory for decades. At the same time, the rodent hippocampus exhibits the salient feature where its principal neurons are active in a spatially selective pattern (i.e., place cell). The place cells change their firing patterns as there are changes in the environments. Until now, we have been interpreting these firing changes, also known as "remapping," to have a functional significance in episodic memory by i) slightly modifying the old map to retrieve subtle changes from the previous memory or ii) forming the new map to reflect any major changes. In the real world, place cells receive complex sensory information from multiple sources, including multimodal sensory inputs and idiothetic information, making it even more challenging to interpret place cell activity from the intermingled sensory inputs fed into the hippocampal system. Taking advantage of the virtual reality (VR) system, I investigated how the hippocampal subregions CA1 and CA3 networks reflect environmental change. Thereby, I parametrically manipulated the environment by adding visual noise (i.e., virtual fog) in the VR environment and examined how hippocampal place cells in the CA1 and CA3 responded as visual noises were added to the environment in a quantified manner. Prior studies have suggested that CA3 forms a discrete

map of the modified environments, presumably by performing either pattern separation or pattern completion. However, place cells in CA1 exhibit less coherent responses to environmental changes compared to CA3. This discrepancy between the CA1 and CA3 subregions is puzzling because CA3 output must pass through the CA1 area before reaching cortical areas. Furthermore, the functional roles of the CA1 in processing the environmental changes still need to be investigated due to the heterogeneous neural outputs with mixed yet conflicting findings. I first questioned whether our VR system reliably induced the place cells from both hippocampal subregions CA1 and CA3. As a result, I observed that the firing properties of hippocampal place cells are equivalent to that reported in the previous studies. Once I confirmed that visual environments in our VR system dominantly controlled the place cells, I examined how place cells in the CA1 and CA3 subregions responded to various levels of changes made to the visual environment. As visual noise was introduced to the familiar environment, I found that place cells in CA1 split simultaneously into two subpopulations: In one, place cells with old maps while changing their firing rate to reflect noise levels (i.e., rate remapping); in another, place cells with new maps to differentiate the dynamically changing environment from an old stable environment (i.e., global remapping). The place cells in CA3 mainly sustained the old map and reflected noise levels by rate remapping. Suppose one considers the rate remapping class of place cells as pattern-completing cells and the global remapping class as pattern-separating cells.

In that case, the CA1 can manifest both pattern separation and pattern completion classes of neurons at the environmental change. My dissertation suggests that CA1 can simultaneously form an orthogonal map of the same environment to remember new episodes without interfering with the old memory.

Keyword : Episodic memory, Hippocampus, Place cell, CA3, CA1, Virtual reality system, Rate remapping, Global remapping

Student Number : 2014-22440

Table of Contents

List of Figures

List of Tables

Background

1. Anatomical structures of the Hippocampal system and their proposed roles

The hippocampus is an archicortical structure conserved across species of mammals, birds, and even in reptiles that is crucial for episodic memory (Allen and Fortin, 2013). Its anatomical differences are distinctive from the neocortex. While the neocortex typically comprises a continuum of six layers and heavily interconnected (Felleman and Van Essen, 1991), the mammalian hippocampus divides into two distinct regions: the Cornus ammonis (CA) and the dentate gyrus (DG), each with three layers of neurons. The connections between hippocampal subregions are primarily unidirectional (Ramon y Cajal, 1893; de No, 1934), in which the information flows from the entorhinal cortex (EC) to the DG to CA3 to CA1 (Andersen et al.,1969), and termed as the "trisynaptic circuit" (Anderson et al.,1969). The function of the hippocampus in episodic memory are based on the anatomical differences between the neocortex and the hippocampus and its unique trisynaptic circuit (**Figure 1**).

The episodic memory is generally viewed as a two-step process: encoding (acquisition) and retrieval (recall). Theories that emphasize episodic memory in the hippocampus have been proposed as the memory traces (i.e., networks) that are effectively encoded and recalled without interference. In this view, episodic memory is supported in the hippocampus

by an auto-associative network in CA3 that stores activity patterns whose redundancy has been previously minimized in the DG. Specifically, the experience or event is represented by activity patterns in the cortex that activate multiple pyramidal neurons in the CA3 (Marr, 1971; O'Reilly and McClelland, 1994; Rolls, 2010).

From the viewpoint of EC as a major information source of the ‘outer world’ to the hippocampus, the superficial layer (II) of the EC first sends the information to the DG, mostly innervating granule cells (Claiborne et al., 1990) via a performant pathway (PP). The Granule cells in DG consist of up to 1000000 cells (Amaral et al., 1990; Boss et al., 1985), significantly diverging from EC input, whereas EC neurons are estimated to be up to 200000 cells (Amaral et al., 1990). Due to the diverging nature of the connectivity (Ramon y Cajal, 1893), the trace for the information is highly separated at this stage. This process is termed pattern separation (Marr, 1971; O'Reilly and McClelland, 1994; Rolls and Kesner, 2006). The sparse and separated trace for the information is then transmitted to the CA3.

The CA3 sends axons to CA1 through the Schaffer collaterals, and the same axons also connect within the CA3 (Gonzales et al., 2001). In rats, 30 ~ 75% of synapses are formed as recurrent collaterals (Ishizuka et al., 1990; Li et al., 1994). These synapses in the recurrent collaterals are strengthened via Hebbian plasticity, forming a memory trace of the event. Therefore, the noisy or partial cortical pattern can recruit a subset of CA3 neurons of the original CA3 pattern associated with the event (Treves and

Rolls, 1992). This process is termed pattern completion (Marr, 1971; O'Reilly and McClelland, 1994; Rolls, 2010). As a partial cue or noisy input enters the system, the neuronal network will eventually retrieve its ensemble patterns through pattern completion, favoring memory retrieval.

The CA1 receives temporoamonic input from the III layer of entorhinal cortex and Schaffer collateral input from CA3 (Amaral and Witter, 1989; Witter et al., 2000). While the CA1 has been considered in associating the CA3 representation of the recalled experience and the EC representation of the original experience (O'Reilly and McClelland, 1994), the CA1 does not have a prominent role from the theory. Yet, based on these anatomical features, it is tempting to speculate that match/mismatch comparison would occur in CA1 (Hasselmo et al., 1996; Lisman and Grace, 2005; Vinogradova, 2001). In this view, if the CA3 representation (i.e., memory) matches the EC representation (i.e., sensory), the hippocampal state will stay in the 'recall mode.' In contrast, if the CA3 representation does not match the original representation of the EC, the hippocampal state will be favored for updating new information. Behavioral experiments raise the possibility that the CA3-CA1 circuit is necessary for mismatch or novelty detection. When the hippocampus is lesioned, the preference for novel stimulus (Honey et al., 1998) or novel place decreases (Lee et al., 2005). Conversely, studies have shown that stimulation of the hippocampus increases exploratory behavior (Flicker and Geyer, 1982; Yang and Mogenson, 1987).

Specifically, this match/mismatch computation is crucial for

processing memory, for the brain has to learn new information distinguished from the already known information. If the brain fails to determine what is previously known, the information will likely interfere with each other. For example, as what we already know interferes with what we are currently learning, someone will not be able to make new memories because of an old one (i.e., proactive interference). On the other hand, someone may also lose track of previously learned content due to new incoming information (i.e., retroactive interference). Despite the importance of match/mismatch computation in the memory process, there is limited empirical evidence from the hippocampal system, especially at the single-unit level.

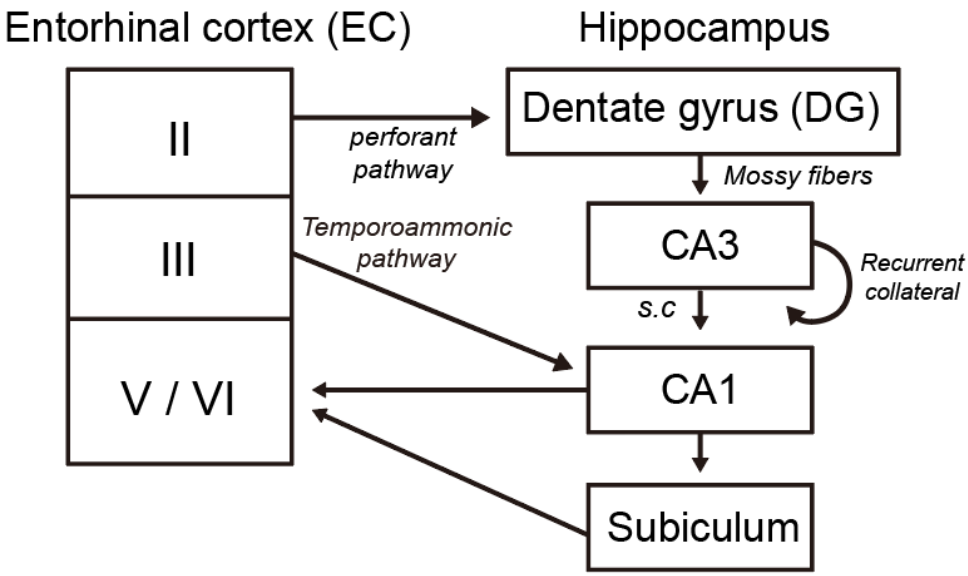

Figure 1. Basic circuit of the hippocampus. The mammalian hippocampus divides into two distinct regions: the *Cornus ammonis* (CA) and the *Dentate gyrus* (DG). The connections between hippocampal subregions are primarily unidirectional, in which the information flows from the entorhinal cortex (EC) to the DG to CA3 to CA1, and termed as the trisynaptic circuit.

s.c: schaffer collateral

2. The remapping properties of Hippocampal place cell

Hippocampal pyramidal cells selectively fire when the animal is in a specific location, termed a place field (O'Keefe and Dostrovsky, 1971). Each place cell has its own spatial receptive fields (i.e., place fields), and the subsets of the place cell represent the distinct cognitive maps for different environments (Colgin et al., 2008; Muller and Kubie, 1987). However, unlike primary sensory cortices, hippocampal place cell representations are not topographically organized (O'Keefe, 1976). A single place cell can induce multiple fields in an environment (Fenton et al., 2008; O'Keefe, 1976; Rich et al., 2014), while other place cells have no fields (i.e., silent) in the environment (Epsztein et al., 2011; Rich et al., 2014; Wilson and McNaughton, 1993). The firing rates of the place field can change dramatically in response to changes in sensory or cognitive input without moving their spatial fields (i.e., rate remapping). Furthermore, place fields can unpredictably change their receptive spatial fields by appearing, disappearing, or shifting (i.e., global remapping). These features of the place cell induced a great challenge when interpreting the causality and the functional significance of the place fields.

The global remapping of the place cell is acknowledged to represent changes in the global geometry, internal variables, or cognitive demands in

the environment. Thus, it is interpreted as coding for the new environment or events. In contrast, rate remapping has been demonstrated to associate with minor environmental sensory changes (Anderson and Jeffery, 2003; Leutgeb et al., 2005b). The rate remapping is observed when there are relatively small environmental changes, such as changing the chamber's color (Fyhn et al., 2007; Leutgeb et al., 2005b). The rate remapping has been interpreted as a coding scheme for reflecting an event and episodes at a particular location because the field firing rates are modulated within the stable place field (Leutgeb et al., 2005).

Since the discovery of the place cell, numerous experiments have been conducted by manipulating visual cues in the recording arena to examine how the place cell representations respond to such changes. The simplest version of such experiments used a polarizing and simple visual cue card in a closed recording arena with the shape of a cylinder (Bostock et al., 1991; Fenton et al., 2000; Kentros et al., 1998; Knierim et al., 1998; Muller et al., 1987; Rotenberg and Muller, 1997; Thompson and Best, 1990) or a box (Wiener et al., 1995). The polarizing visual cue card could be rotated around the walls of the arena (Knierim et al., 1998; Muller and Kubie, 1987), reduced to half in size, or removed from the recording arena (Muller and Kubie, 1987). The results from those earlier studies strongly demonstrate the powerful influence of the visual cue on the positional firing patterns of place cells. In this typical foraging experiment, the animals usually experienced simple visual cues with simple geometric boundaries.

However, the demonstration of the almost perfect control over place fields by the polarizing visual cue in the cylinder or box environment might be exaggerated due to the oversimplified environment. Also, it has been unclear whether the cue card always serves as a distal cue because it can become a proximal (or even tactile) cue when the animal gets closer to the cue in the arena. This question may have led researchers to manipulate individual cues in a more complex environment with multiple stimuli (and presumably the patterns evoked by those stimuli) allocentrically provided as spatial cues.

From the late 1990s to early 2010, numerous research had been bloomed to find the functional implication of hippocampal place coding by altering the environment. Specifically, the most frequent manipulation has been to alter the surrounding allocentric environment, or sensory experience of an animal by using a double-rotation paradigm (Lee et al., 2004; Shapiro et al., 1997; Tanila et al., 1997), morphed geometry conditions (Colgin et al., 2010; Leutgeb et al., 2005a; Wills et al., 2005), sensory cue change in the foraging arena (Anderson and Jeffery, 2003; Leutgeb et al., 2005b; Save et al., 2000). There were multiple distal cues attached to the curtains that surround the maze (Hetherington and Shapiro, 1997), sometimes in combination with olfactory or tactile cues (Knierim and Rao, 2003; Shapiro et al., 1997; Tanila et al., 1997). These prior studies have reported that place cells in the hippocampus represent not only some salient landmarks in the environment but also the configural relationships among the multiple stimuli

in the environment. Overall, it turned out that the hippocampal place cells react to environmental manipulation more complexly than we had expected. For example, at the change of the environmental change, or events in the same environment, the split of rate remapping and global remapping cells has been observed in the previous literature as partial remapping (Anderson and Jeffery, 2003)

Furthermore, the hippocampal firing patterns are determined not only by the stimulus configurations in the environment but also by some internal variables such as idiothetic information (Ferbinteanu and Shapiro 2003), task demand (Bahar and Shapiro, 2003; Bahar and Shapiro, 2011; Park and Lee 2016; Lee et al.,2018; Aronov et al.,2017; Markus et al.,1995), and motivational states (Eichenbaum, 2000; Ferbinteanu and Shapiro, 2003; MacDonald et al., 2011; Markus et al., 1995). For example, when the rat foraged in two visually identical chambers connected by a corridor, the spatial representations of the place cells for the two chambers differed from each other (Skaggs and McNaughton, 1998).

Among the numerous literature that reports the place field dynamics in the hippocampus, there has been a large consensus that the CA3 displays more coherent firing patterns than the CA1 at the environmental modification or any environmental events (**Table 1**). Specifically, prior studies have suggested that CA3 is important in processing environmental changes, presumably by performing either pattern separation or pattern completion (Lee and Lee, 2020; Lee et al., 2004; Leutgeb et al., 2005;

O'Reilly and McClelland, 1994). Furthermore, even with the changes in the internal variables, CA3 tends to maintain its place fields most of the time.

In contrast, place cells in CA1 exhibit less coherent responses to changes in the sensory environments as well as internal variables in the same environment compared to this in CA3 (Lee et al., 2004; Leutgeb et al., 2005; Vazdarjanova and Guzowski, 2004; Bahar and Shapiro 2011). Moreover, the partial remapping of place cells in response to environmental change seems more common in CA1 than in CA3 (Lee et al., 2004; Leutgeb et al., 2005b) (**Table 1**). Therefore, the functional roles of the CA1, which is the primary cortical output of the hippocampal circuit, remain largely unknown due to the heterogeneous neural outputs with mixed yet conflicting findings (Colgin et al., 2010; Wills et al., 2005).

Specifically, both studies tested the neural outputs of CA1 across the morphed geometry between the square and circle environments (Colgin et al., 2010; Wills et al., 2005). Wills et al. reported an acute transition of the spatial representation at the specific morphed condition (i.e., global remapping), whereas Colgin et al. reported the gradual remapping along with the morphed conditions (i.e., partial remapping). One of the factors that contributed to the conflicting findings from prior studies is the different experimental protocols as well as conditions used among different studies. This discrepancy was later demonstrated to be produced by individual animals' prior experience (Colgin et al., 2010; Plitt and Giocomo, 2021). Yet, the meaning of the partial remapping in CA1 for processing environmental

modification still needs to be determined.

(**Table 1**)

Double-rotation paradigm:

Study	Manipulation	Remapping patterns	Subregion
Shapiro et al., 1997	Double-rotation paradigm (sensory conflicts between local cue vs. distal cue)	After the sensory conflict, the place fields were found to be following (i) local cue or distal cue: concordant, or showed complex pattern (ii) to be classified as a discordant cell (i.e., appear; disappear; mixed)	**CA1**&**CA3** (new field representation: 50%)
Tanila et al., 1997			**CA1** (new field representation: 40%; stable:10%; concordant: 50%)
Tanila et al., 1998			**CA1** (concordant: 37%)
Lee et al., 2004b			**CA1** (concordant: 27%; discordant: 73%) **CA3** (concordant: 60%; discordant: 40%)

Sensory cue change:

Study	Manipulation	Remapping patterns	Subregion
Save et al., 2000	Light on/off; floor cleaning/ not cleaning for the local cue	Place fields remained more stable at the presence of the local cue (i.e., no cleaning condition) in the light-off condition	**CA1** & **CA3** (stable: 80%; no light & local cue) **CA1** & **CA3** (stable: 9%; no light & no local cue)
Hayman and Jeffery 2003	Wall color change; different box position (i.e., North vs. South)	Heterogeneous remapping in CA1 was observed	**CA1**
Anderson and Jeffery 2003	Wall color change; odor stimuli change		**CA1**
Leutgeb. S et al., 2005	Wall color change; geometry change	Orthogonal representations in CA3; gradual changes in CA1 were observed	**CA1**; **CA3**
Fetterhoff et al., 2021	visual pattern switch	The authors speculate the hippocampal remapping by a 'hidden state' of an animal (Sanders et al.,2020)	**CA1**

(**Table 1** continued)

Morphing geometric environments:

Study	Manipulation	Remapping patterns	Subregion
Leutgeb JK et., al 2005	Morped geometry conditions across square vs. circle	Gradual remapping across the morphed conditions in CA1; Acute differentiation of spatial representation at the certain point of conditions in CA3	Different dynamics of **CA1** (i.e., acute vs. gradual) across the morphed conditions were observed across the studies
Wills et al., 2005		Acute differentiation of spatial representation at the certain point of conditions in CA1	
Colgin et al., 2010		Gradual remapping across the morphed conditions in CA1; relatively acute remapping at the certain point of conditions in CA3	
		Acute differentiation of spatial representation at the certain point of conditions in CA1; Acute differentiation of spatial representation at the certain point of conditions in CA3	
Plitt and Giocomo 2021	visual pattern morphing; prior experience	The remapping in the CA1 is differed by prior experience of morphing patterns	**CA1**

(**Table 1** continued)

Remapping by internal variables:

Study	Manipulation	Remapping patterns	Subregion
Moita et al., 2004	Electric shock	Decreased spatial correlation in CA1 within the same box after experiencing an electric shock	CA1
Wang et al., 2012	Coyote odor	Quantified remapping cell proportion in CA1 after experiencing the coyote urine	CA1 (stable cells: 58%; remapping cells: 42%)
Kim et al., 2015	Predatory robot	Remappings were found to be more prominent nearby a 'predatory robot'	CA1
Ferbinteanu and Shapiro 2003	goal location switch	Journey dependent place cells with different fields position on the plus maze	CA1
Bahar and Shapiro 2011	Task rule switch	Different remapping proportions at the task rule switch on the plus maze	CA1 (stable: approximately 30%; remapping & binary: approximately 70%) CA3 (stable: approximately 55%; remapping & binary: approximately 45%)
Park and Lee 2016	curtain configuration (AMB)	Increased variability in the place fields at the introduction of additional curtain configuration in the distal cue-based memory task	CA1&CA3 (stable: 74%; dissimilar: 26%)
Lee et al.,2018	Blurred scene on the t-maze screen	Significantly rate modulated place cells in CA1 after the introduction of blurred scene on the t-maze screen	CA1 (stable: 25%; significant rate modulation: 75%)
Okada et al., 2017	Air puff	Remappings were reported in CA1 after experiencing an Air-puff	CA1 (stable: 40-50% on the air-puff arm; stable: 20%-35% on the other side of an arm with no air-puff)
Markus and Barnes 1995	Task contigency	Distinct quality of place fields across diffent task contigency	CA1&CA3 (Approximately a one-third of the population showed a remapping)
Aronov et al., 2017	Task contigency		CA1

3. The usage of the virtual reality (VR) system for rodents in studying the hippocampus

One of the caveats of recording hippocampal place cells in freely moving animals is that the animal subject, instead of the experimenter, controls where to look and what to sample. Consequently, it has always been challenging to manipulate an animal's sensory experience. Interpreting the less coherent CA1 activity had been complicated due to the sensory inputs fed into the hippocampal system being largely unknown in most cases. It seemed nearly impossible to control the sensory stimulus fed to the hippocampus until the VR systems for rodents were introduced to the rodent experimental paradigm in the early 21st century (Harvey et al., 2009; Holscher et al., 2005). In a typical rodent VR system, the animal subject runs on a treadmill or ball with its head or body on the treadmill or ball while the visual patterns projected to the surrounding screens change as a result of the animal's locomotive movement.

The rodent VR system has the enormous advantage of removing intermingled sensory inputs other than visual stimuli, such as tactile and vestibular inputs, and allowing the parametric manipulation of visual patterns. In the last two decades, rodent VR studies have shown that rodent behavior is more visual than previously thought (Holscher et al., 2005; Sato et al., 2017; Youngstrom and Strowbridge, 2012). Moreover, a growing number of studies have implied that visual patterns alone can drive the

spatial information processing of hippocampal networks to a sufficient level compared with real-world situations (Bourboulou et al., 2019; Cohen et al., 2017; Priestley et al., 2022; Ravassard et al., 2013).

The ability to control the allocentric visual environment in a precise and parametric way in the VR system opened the possibility of testing traditional computational models in the hippocampal research field more rigorously than in real-world experimental settings. That is, computational models can provide precisely controlled input patterns and their modified forms to the hippocampal network during simulation (Churchland and Sejnowski, 1992; O'Reilly and McClelland, 1994; Treves and Rolls, 1994), but it has been difficult to experimentally test such results, mainly because the exact nature of input patterns sampled by the animal is often unknown in a traditional experimental setting. When testing the computational principles of the network (e.g., pattern completion and pattern separation) in the hippocampus, the visual stimuli in the environment can be systematically manipulated to feed noisy or degraded inputs to the network. A similar emphasis on the importance of testing degraded input patterns in testing hippocampal networks has been made, especially since the three important physiological findings were made (Varzdajzanova and Guzowski, 2004; Lee et al., 2004; Leutgeb et al., 2004). However, traditional experimental paradigms in the real world can only perform the latter (i.e., partial inputs) by removing some of the environmental cues (Gold and Kesner, 2005; Nakazawa et al., 2002), but not the former (adding noise). Furthermore,

despite the theoretical importance of testing the network's behavior with noisy input patterns, until these days, it has been almost impossible to create an experimental condition to add parametrically quantifiable noise to the environment in real experimental settings.

In contrast, adding sensory noise (e.g., virtual fog) to the virtual world is relatively easy. The noise level can also be controlled in a parametric way to examine the functional relationships between environmental changes and the physiological responses of hippocampal neurons. Using the VR experimental setup, my thesis has introduced a controlled manner to explore the hippocampal networks with sensory noise added to the original environment in a parametric fashion for the first time. This opened up a new possibility for interpreting the neural responses of the hippocampal subregions at the environmental modification, especially for elucidating the complicated remapping patterns found in CA1.

Nevertheless, while the VR system allows the direct comparison of the place cell responses to precisely controlled visual stimuli, it lacks certain components of the real-world experimental settings, such as the simultaneous experience of multiple sensory modalities and the presence of vestibular inputs, which could be a potential limitation.

Chapter 1. Visual scene stimulus exerts dominant control over the place fields in the virtual reality system

Introduction

The hippocampus plays a crucial role in spatial memory and navigation by forming a cognitive map of the environment (O'Keefe and Nadel, 1978). Place cells in the hippocampus are considered the building blocks of cognitive maps because they fire in specific locations (O'Keefe and Dostrovsky, 1971). Changes in the spatial representations (i.e., remapping) of place cells are taken as neural evidence for coding a modification to the environment (Muller and Kubie, 1987). Place cells in the hippocampus tend to exhibit “global remapping” for significant environmental changes (e.g., moving to a different room) by shifting their place fields to different locations or turning on/off their activities (Bostock et al., 1991; Thompson and Best, 1989). For small environmental changes, however, place cells tend to show “rate remapping”, in that they fire in their original fields but change their firing rates to code the sensory modifications (Allen et al., 2012; Lee et al., 2018). However, interpreting the place cell remapping has not been straightforward due to the complicated sensory inputs fed into the hippocampal system being largely unknown in real-world settings. To investigate the hippocampal place cells in a more controlled fashion, I constructed a virtual reality system for the head-fixed rats that is compatible with *in vivo* electrophysiology.

In this part of the thesis, I first validated the place cell activity from our virtual reality system. The validation of the place cell is essential in this

chapter, for my primary goal is to test the behavior of the place cells in visually modified environments. To confirm whether place cells are visually induced in the virtual environments, I recorded single units from CA1 and CA3 while the animals experienced each environmental setting and compared the basic firing properties to the previously reported studies. I verified whether the place cells induced in the virtual environments were comparable to those reported in real-world foraging conditions. Furthermore, I created the conditions where the body movements were decoupled from the visual stimulus (i.e., sensory-motor gain manipulation) or auditory contexts (i.e., auditory contextual switch manipulation) to test the dependency of the visual scene in the place cells.

Materials and methods

Subjects

Male Long-Evans rats (n = 8) weighing 400–500 g were used. After rats had fully recovered from surgery, water was restricted to maintain the animal's body weight at ~85% of its free-feeding weight. Food was available ad libitum. Animals were housed individually under a 12-hour light/dark cycle. The experimental protocol complied with the guidelines of the Institutional Animal Care and Use Committee of Seoul National University.

Surgery

After undergoing a handling session, rats were implanted with a hyperdrive carrying 24 tetrodes and three reference electrodes for simultaneously recording single-unit spiking activities from the dorsal CA1 and CA3. Prior to surgery, the animal was first anesthetized with an intraperitoneal injection of sodium pentobarbital (Nembutal, 65 mg/kg), after which the animal's head was fixed in a stereotaxic frame (Kopf Instruments, USA). Isoflurane (0.5-2% mixed with 100% oxygen) was used to maintain anesthesia throughout the surgery. For local analgesia, benzocaine was sprayed onto the scalpel blade before an incision was made along the midline of the skull. The hyperdrive was targeted to the right dorsal hippocampus (3.6-4.0 mm posterior to bregma; 3.0-3.6 mm lateral to the midline). In four rats, I also

implanted a tetrode-carrying bundle over the visual cortex (lateral extrastriate visual cortex; V2L) to simultaneously monitor single-unit activities in that region along with those in the dorsal hippocampus. The tetrode bundle for the visual cortex was implanted to cover the V2L in the right hemisphere (6.5 mm posterior to bregma, 6.0 mm lateral to the midline). A custom-made acrylic head-mount structure, cut using a CNC milling machine (Nomad 3; Carbide 3D), was implanted above the skull to secure the animal's head in the VR system **(Figure 3)**. The hyperdrive and head-mount structure were chronically affixed to the target area by multiple skull screws peripherally placed on the skull using bone cement. After surgery, ibuprofen syrup was administered orally for general pain relief. The animal was kept in an intensive care unit overnight, with temperature and humidity maintained using a controlled system.

VR system

I constructed the custom VR experimental system using a game engine [*Unreal Engine 4.14.3*; (*Epic Games, Inc*)] **(Figure 2)**. Rats were head-restrained to run at a constant position on a Styrofoam cylinder (66 cm in diameter and 20 in width). A piece of a commercial yoga mat was applied to the surface of the cylinder to provide appropriate friction during running. An optical sensor attached to the supporting frame detected and measured the rotation of the cylinder. The VR environment was controlled by the signal

transmitted from the optical sensor to the Unreal Engine in association with the rat's movement. Three 24-inch LCD monitors were placed to cover approximately 270° (-15° to +25° of elevation) of the rat's field of view. A licking port was placed in front of the rat's snout to provide a water reward when the rat licked the port. The solenoid valve was controlled by the UE via an Arduino interface board so as to provide a fixed amount of water. For each frame of the UE, the Arduino interface triggered a TTL signal. The signal was sent to the data acquisition system for synchronization of timestamps generated by the two systems.

Dilation of the rat's pupil was measured during the behavioral session by monitoring the animal's eye using a CCD camera (eco204CPGE, *SVS-VISTEK*, 1024 · 776 pixels) equipped with a manual zoom close-up lens (MLH-10x; Computar) with an infrared filter (UV/VIS Cut-off M46.0 · 0.75 Machine Vision Filter; Edmund Optics) while the animal's left eye was illuminated with an infrared light source (S-IR5850; Skycares). The camera was aligned to a 45° angle relative to the midsagittal axis of the animal. Image data were acquired in response to the TTL signal triggered by each frame of the Unreal Engine.

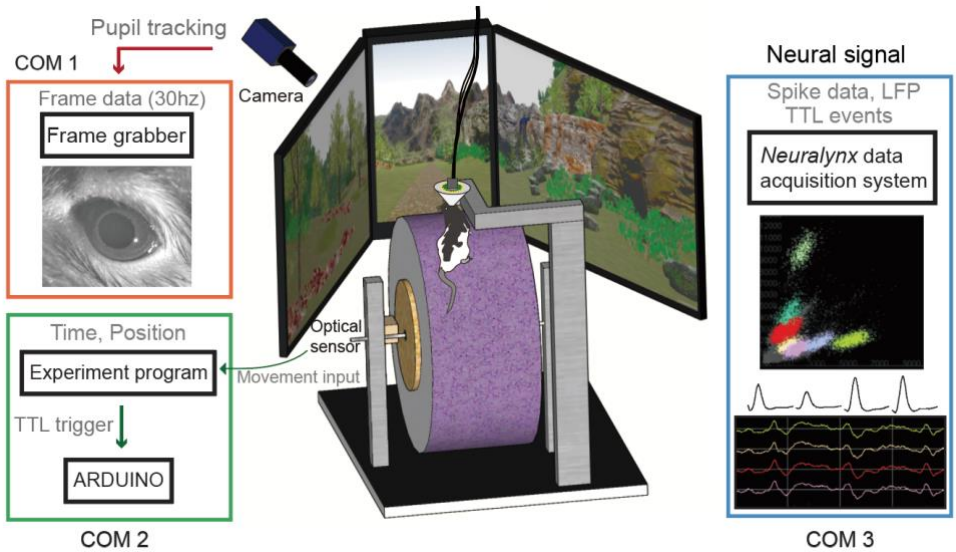

Figure 2. VR setup. The virtual reality system was designed for head-restrained rats (n = 8) using a game engine, *Unreal Engine*. The rotation of the Styrofoam cylinder was measured by an optical sensor attached to the side of the cylinder, and a rolling signal controlled the movement in the virtual environment. The head-fixed rats on a treadmill navigated the virtual environment projected through three surrounding LCD monitors. Water was delivered through the reward port, and rats were required to move forward on a linear track within the virtual environment to obtain rewards at the randomized location. The cell activity was recorded through a hyperdrive connected by tethers. Here, I monitored the neural activities of the place cells and pupil behaviors during the data acquisition sessions.

Electrophysiological recording

After allowing one week for recovery from surgery, tetrodes were gradually lowered to the dorsal CA1 and CA3. Tetrodes were adjusted while the animal rested on a circular platform on a pedestal in a soundproof booth outside the behavioral testing room. Neural signals were transmitted to a data acquisition system (Digital Lynx SX, Neuralynx) through a headstage (HS-36, Neuralynx) connected to an electrode interface board (EIB-36-24TT, Neuralynx) attached to the hyperdrive. Neural signals were digitized at 32 kHz (filtered at 600–6,000 Hz) and amplified 1,000–10,000 times. Tetrodes were lowered daily by small increments to maximize recording yields per tetrode.

Behavioral pre-training in the VR system

After recovering from surgery for one week, rats' free access to water was restricted to maintain their motivation level for water. Specifically, the water motivation level for each rat was monitored as the animal freely foraged on a cart for water drops provided by the experimenter through a handheld syringe. Based on the rat's behavior during testing, I provided various amounts of water (from 1 to 5 mL) over time. Food was available *ad libitum*. Once the animal manifested a high level of motivation for water, I head-fixed the animal in the VR system for a 30-minute familiarization session, during which the rat ran along a virtual linear track (3-meter in length) with

a gray-scaled 2D visual scene. At the end of the track, a tunnel (0.5-meter in length) appeared. When the rat entered the tunnel, it experienced a completely dark environment with no visual stimuli except the light at the end of the tunnel exit. When the animal reached the end of the tunnel, the UE program virtually teleported the rat back to the start of the track to experience the same environment while running on the linear track. The purpose of the familiarization session was to train the rat to run along a linear track to obtain water rewards at two random sites (20 μL/site) on the track per trial. The main data-acquisition schedule began once the rat ran more than 300 m in 30 minutes on two consecutive days.

The experimental settings and recording schedules

Standard recording session

Two visually enriched environments—Forest and City—were created for testing place cell behavior in a cue-rich environment (**Figure 3**). Each environment was constructed so as to mimic a complex and natural visual environment with contextually relevant visual landmarks and objects along the entire track.

In addition, auditory cues were provided in some areas of the VR environment. For example, a realistic waterfall sound was audible by the rat as the rat passed the waterfall in the environment. The two VR environments were provided in a blocked fashion (e.g., Forest-City-Forest-City-Forest; at

least 10 trials/block) or in a pseudorandom sequence (30 trials per environment). Once the rat reached the end of the 3-m track, it experienced a tunnel (0.5 m in length) before encountering the next environment (either the same or different environment depending on the recording schedule). Single units were recorded simultaneously while the rats (n = 8) experienced the VR environments. The main recording period for the standard session lasted 4 days. Afterward, single units were recorded while the familiar VR environments were altered (a) by manipulating auditory stimuli associated with the visual scenes and (b) by manipulating sensory-motor gain. Details of each environmental manipulation are as follows:

(a) Auditory context switch - In the auditory contextual switch session, the auditory stimuli used in one environment (e.g., Forest) were presented in the other environment (e.g., City) in the middle of the session, thus causing incongruences between visual and auditory contexts. For example, auditory context A was introduced in the visual environment B (or vice versa) during the session's 3rd block and 4th block. Each session consisted of six consecutive blocks of ten trials.

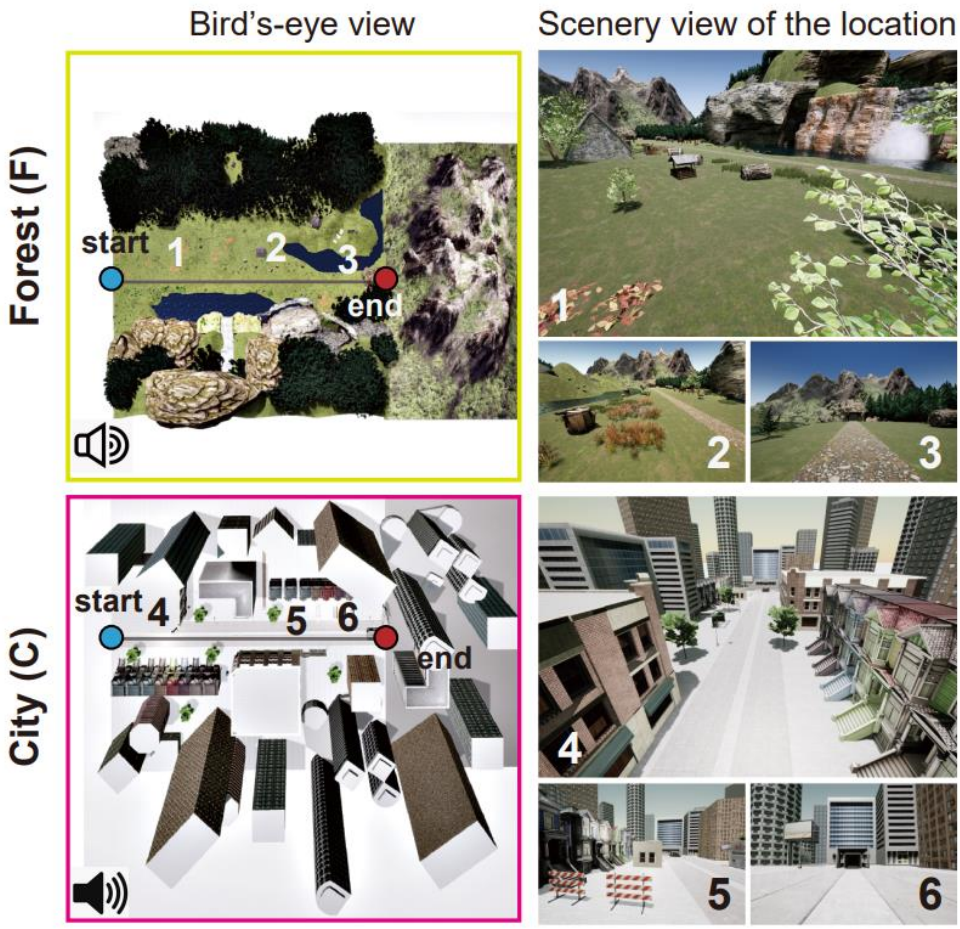

Figure 3. Two visually enriched virtual environments. (*Left*): Bird's-eye views of the environments. Forest consisted of trees, rocks, and waterfalls, and the sounds relevant to the corresponding location (e.g., grass bugs, waterfall) were played as the auditory context. In City, various shapes of buildings were installed, and the sounds relevant to the location (e.g., city noise, people chattering) were played as the auditory context. Rats ran through the linear track in the middle of each environment, represented by a horizontal line between the start (*blue*) and end (*red*) circles. (*Right*): Screen-captured scenes of the corresponding places on the left column.

(b) *Sensory-motor gain manipulation* - In the gain-manipulation session, rats experienced >10 consecutive trials as a baseline. Trials in which the gain between the visual environment and movement increased twice ("2x gain" trials) were then introduced in a pseudorandom sequence. In 2x gain trials, rats advanced twice the distance in the VR environment compared to the standard condition.

Histology

After the completion of all recording sessions, the animal was sacrificed by inhalation of an overdose of CO_2 and then was transcardially perfused first with phosphate-buffered saline using a syringe and then with a 4% v/v formaldehyde solution using a commercial pump (Masterflex Easy-Load II Pump; Cole-Parmer). The brain was extracted and soaked in 4% v/v formaldehyde-30% sucrose solution at 4°C for ~3–4 days until it sank to the bottom of the container. After post-fixation procedures, the brain was gelatin-coated and soaked in 4% v/v formaldehyde-30% sucrose solution for one more day. The brain was sectioned at 40 μm using a freezing microtome (HM 430; Thermo-Fisher Scientific), and brain sections were mounted on subbed slide glasses and stained with thionin. Visual cortices were identified by additionally performing Timm staining on every other section. Photomicrographs of brain tissues were taken using a digital camera (Eclipse 80i, *Nikon*) attached to a microscope. Tetrode tracks were reconstructed from histological photomicrographs, the original bundle

design of the hyperdrive, the depth profiles of the recording during data acquisition, and the rat atlas (Paxinos and Watson, 2009) **(Figure 4)**.

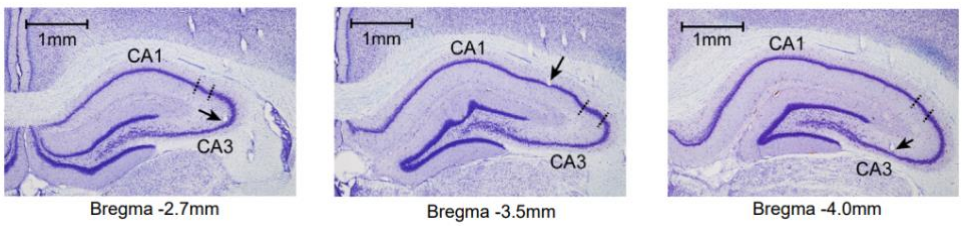

Figure 4. Recordings of CA1 and CA3 place cells with tetrodes. Simultaneous recording of single-cell activity from CA1 and CA3. Photomicrographs of Nissl-stained tissue sections showing tetrode trajectories in CA1 and CA3. Black arrows indicate the locations of tetrode tips. Dotted lines are boundaries between CA1, CA2, and CA3 subregions. Scale bar: 1 mm.

Unit isolation

Single units were isolated offline with custom-written software (*WinClust*) using the peaks and energy values of individual spikes as major criteria. Details of unit-isolation methods can be found in our previous studies (Delcasso et al., 2014; Lee and Kim, 2010). For analysis, we included only well-isolated clusters in which the proportion of spikes recorded during the refractory period was less than 1% of the total spikes of a single unit. Cells with an overall mean firing rate less than 6 Hz and a peak-to-valley width exceeding 150 μs were classified as pyramidal neurons. Among these pyramidal neurons, cells with a mean firing rate greater than 0.5 Hz in at least one condition of the recording session were counted as valid units and were included in subsequent analyses.

Data analysis

Running velocity calculation and data filtering

Position data in the VR system were acquired at a 30 Hz sampling rate. The instantaneous velocity of the animal was calculated as follows:

$$v_i = (p_{i+1} - p_i) \times (Sampling\ rate)$$

where i denotes the position in the ith frame of the acquired data, and v_i and p_i denote the instantaneous velocity and position in the ith frame, respectively. Instantaneous velocity was smoothed using a moving average

method (window size = 0.5 seconds). Neural activity during sharp-wave ripples was filtered out by excluding data in which the instantaneous velocity was less than 3 cm/s.

Rate map construction

For the construction of the rate map, the 3-m long track was divided into 100 bins (bin size = 3 cm) and then the firing rate of each bin was calculated by dividing the number of spikes by the duration of occupancy for the bin. The adaptive binning method (Skaggs and McNaughton, 1993) was then used to smooth the raw rate map.

Quantification of spatial properties

The amount of spatial information conveyed by a single neuron was measured by computing the amount of spatial information carried by a single spike of the neuron using the following equation (Skaggs and McNaughton, 1993):

$$Spatial\ information\ score = \sum_i p_i \frac{\lambda_i}{\lambda} log_2 \frac{\lambda_i}{\lambda}$$

where i denotes the ith bin, p_i is occupancy rate in the ith bin, λ_i is the mean firing rate in the ith bin, and λ is the overall mean firing rate. The mean firing rate was obtained by averaging the firing rates in the raw rate map. Prior studies (Markus et al., 1994) showed that the spatial information of a place cell could be biased by the cell's firing rate. Since the neural activity levels

were influenced by the nature of the visual stimuli in our study, I tested the statistical significance of spatial information for each neuron. Specifically, I generated a surrogate rate map in which the timestamp series of spikes were shifted forward or backward by a random amount to produce a distribution of spatial information from the surrogate data (Acharya et al., 2016; Markus et al., 1994; Ravassard et al., 2013). Then, the spatial information distribution was used to determine the significance of our spatial measures ($p < 0.001$), including spatial information. The spatial information score was then calculated from the surrogate rate map. This process was repeated 1000 times, yielding a distribution of spatial information scores of the surrogate rate maps. The *p*-value was the surrogate spatial information score ratio that exhibited a higher value than the actual spatial information score.

In the current study, cells that satisfied the following three criteria were classified as place cells: (i) mean firing rate > 0.5 Hz, (ii) spatial information > 0.1 (bits/s), and (iii) p-value of spatial information < 0.001. In addition to the spatial information score, the area occupancy of spikes throughout the track (an indication of how focal the firing of a cell is on the track) was quantified by measuring the sparsity of the rate map, a metric that has been used in addition to the spatial information score as an index for the spatial activity of a cell. Sparsity was computed using the following formula (Skaggs et al., 1996):

$$Sparsity = \frac{(\sum p_i \lambda_i)^2}{(\sum p_i \lambda_i^2)}$$

where the same symbols were used as in the formula for calculating spatial information above. To minimize the effect of the animal's behavior on the measurements, I assumed that p_i in the sparsity formula was uniformly distributed in the maze (Jung et al., 1994).

Detection of place-field boundaries

In the current study, the spatial firing pattern of a single unit was operationally defined as a "place field" if five or more contiguous bins exhibited firing rates that were more than 15% of the peak firing rate in the unit's spatial firing rate map. Boundaries were detected as points in a place field where the place cell's peak firing rate was greater than 1 Hz. If there was another peak exceeding 50% of the peak firing rate after the first cycle of the field detection algorithm, an additional cycle was run to detect an extra field using the same thresholding algorithm used to detect the field.

QUANTIFICATION AND STATISTICAL ANALYSIS

Data were statistically tested using a custom program written in MATLAB R2020a. I used Chi-square test, Wilcoxon rank-sum, Wilcoxon sign-rank test, Kruskal-Wallis test, Kolmogorov-Smirnov test, and analysis of variance (ANOVA) to determine the statistical significance when appropriate. The Chi-square test was used for proportional comparisons. A Wilcoxon rank-sum test was applied to compare firing rates or spatial information scores across the different, visually manipulated conditions or between different subregions. I used Wilcoxon sign-rank tests to test the behavioral differences or field sizes from each environmental condition. The significance of the difference between the groups was determined using the Kruskal-Wallis test, Wilcoxon rank-sum test, or Kolmogorov-Smirnov test when normality could not be assumed. ANOVA was used to analyze the effects of the fog condition and subregions CA1 and CA3. Unless otherwise indicated, the significance level was set at $\alpha = 0.05$. All error bars indicate the standard error of means (SEM).

Results

Place cells fire more orthogonally for different environments in CA3 than in CA1

I constructed two visually enriched environments, each composed of unique visual landmarks, objects, and background scenes (Forest and City; **Figure 3**). Adjacent trials were separated by the presence of a virtual tunnel. I recorded single units simultaneously from both CA1 (n = 576) and CA3 (n = 546) from eight rats while they ran in the VR environments. I first verified that the behavior of rats, measured as velocity, was fairly homogeneous between the two VR environments (n = 30, Z = -0.96, p = 0.34; Wilcoxon signed-rank test) (**Figure 5**). Place fields that fired in only one of the VR environments were observed robustly in both CA1 (**Figure 6A**) and CA3 (**Figure 6B**), although some cells fired in both environments (CA1 cells *526-02-11-4*, *536-04-13-1* in **Figure 6A**).

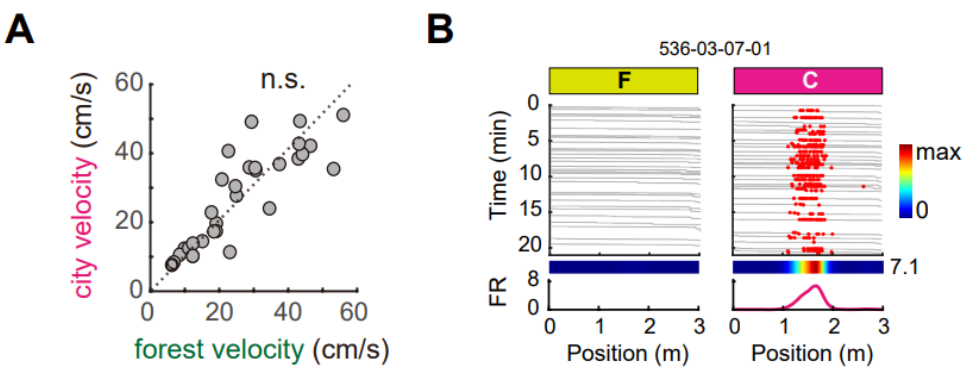

Figure 5. Averaged velocity and the place cell activity in the virtual environment. (A): The rats (n = 8) exhibited comparable velocity within each environment with no bias in the running behavior in the specific

environment (3-4 sessions / rat). (B): The representative example of place field.

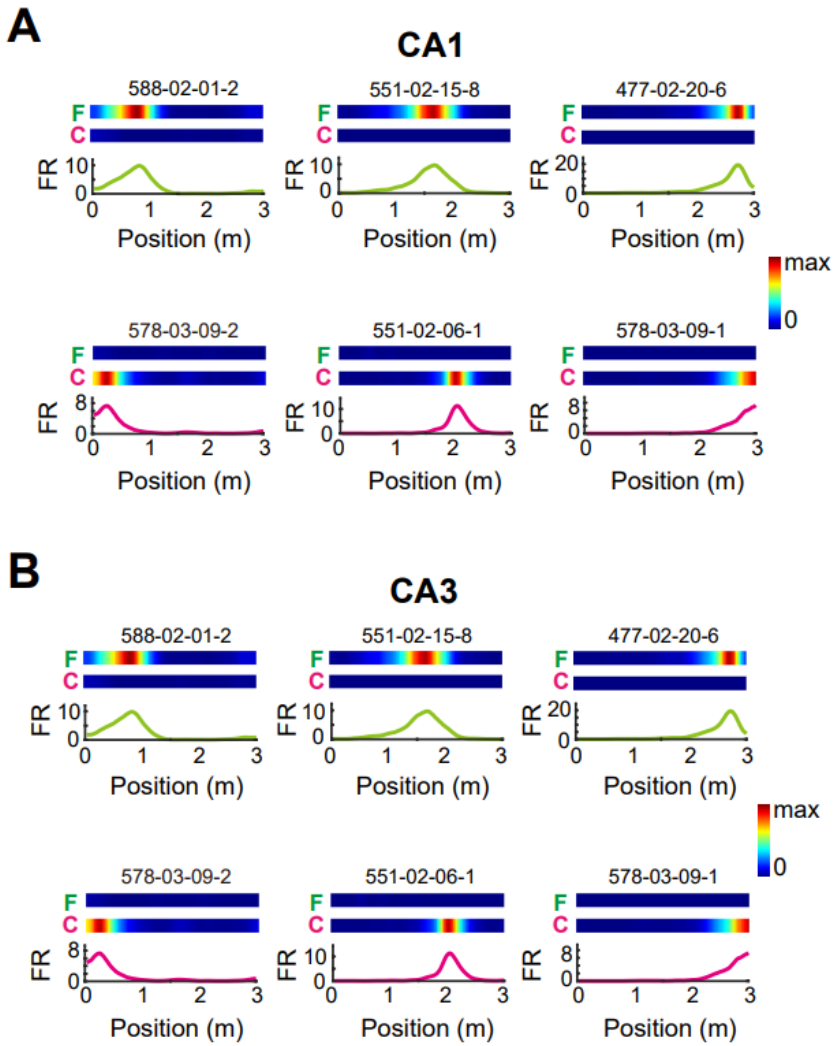

Figure 6. Representative examples of place fields from the City and Forest, respectively. The typical place fields along the linear track of the virtual environments were observed from (A) CA1 (B) and CA3. Most of the place cells showed an environmental-specific firing pattern.

Place cells were predominantly controlled by the visual scenes, as altering idiothetic information generated from the animal (**Figure 7**; **Figure 8**) or auditory associated with the visual environment had negligible effects on neural activity (**Figure 9**; **Figure 10**).

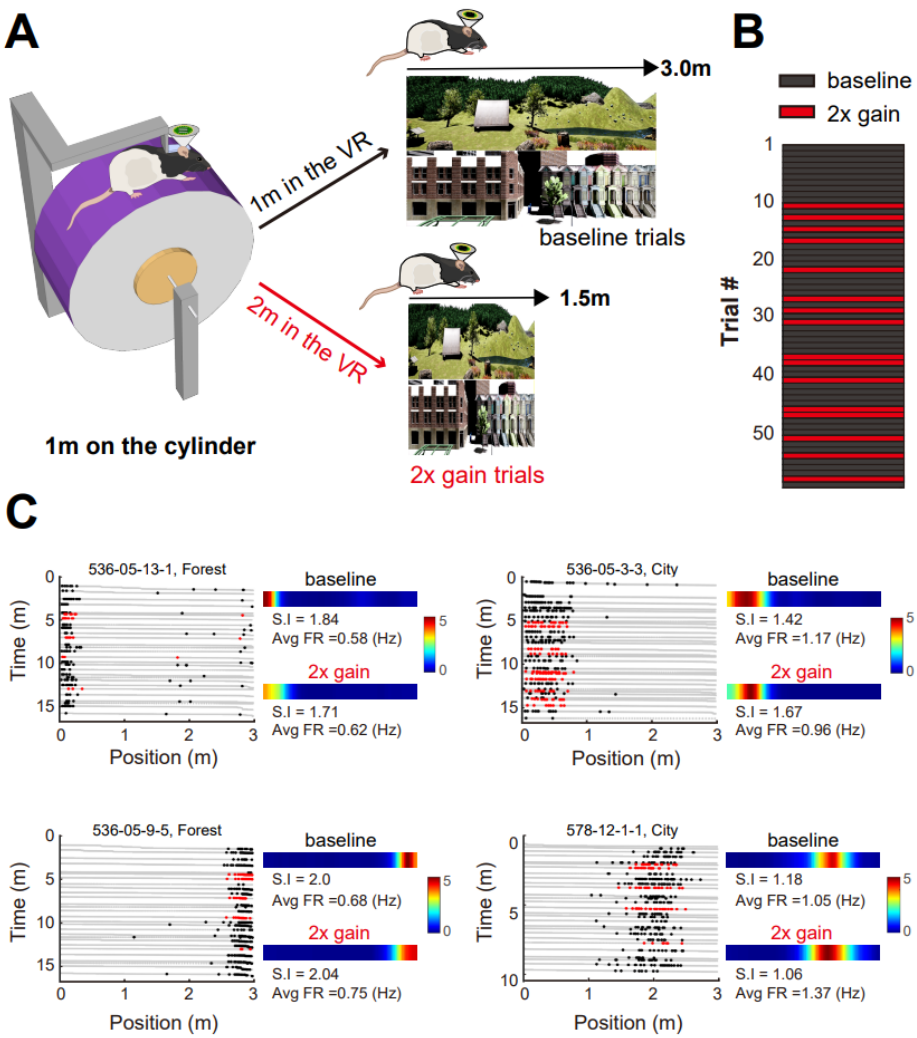

Figure 7. The sensory-motor gain manipulation. (A): Schematic illustration of sensory-motor gain manipulation. In 2x gain trials, rats advanced twice the distance in the VR environment compared to the

standard condition. (B): Representative examples of trial sequences of 2x gain trials (*red*) intermixed with baseline trials (*gray*) in a session. The number of 2x gain trials was equal between the VR environments (i.e., Forest and City). In the gain-manipulation session, rats experienced >10 consecutive trials as a baseline. Trials in which the gain between the visual environment and movement increased twice ("2x gain" trials) were then introduced in a pseudorandom sequence. (C) Representative place cells from gain-manipulated sessions. Black dots (baseline) and red dots (2x gain) indicate the raw spiking activities for individual trials in the session. Two average rate maps constructed based on baseline trials and 2x gain trials were generally similar to each other. Spatial information (S.I.) and averaged firing rates are given below each rate map.

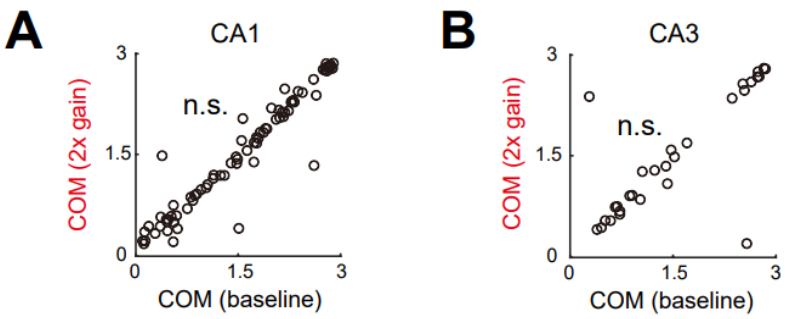

Figure 8. Center-of-mass (COM) from both baseline and 2x gain conditions for individual place fields. No significant differences in COM between baseline and 2x gain conditions were found in (A) CA1 (n = 102) (p = 0.6565; Wilcoxon signed-rank test) or (B) CA3 (n = 78) (p = 0.7499; Wilcoxon signed-rank test).

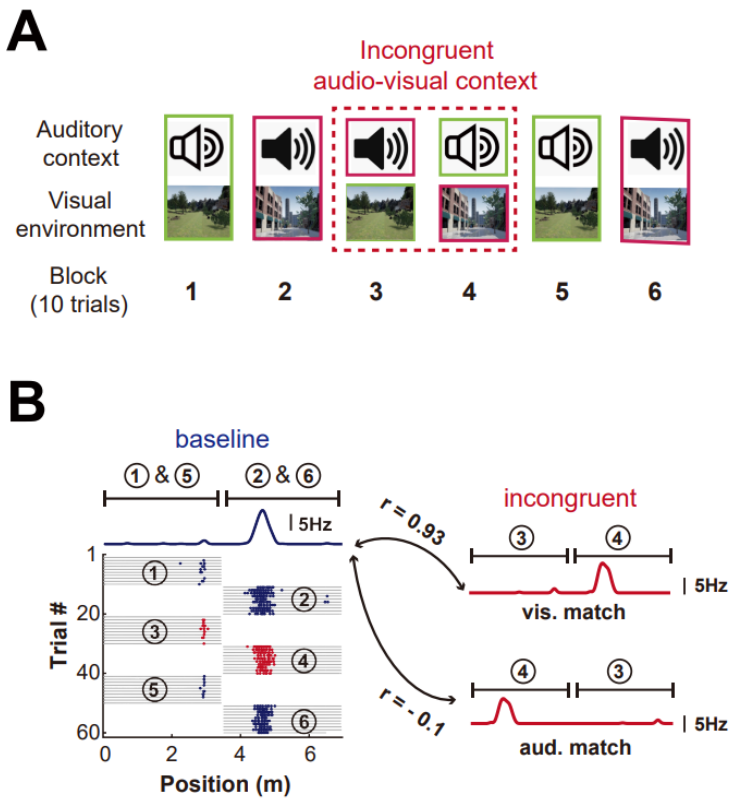

Figure 9. The auditory contextual switch manipulation. (A): Schematic illustration of the auditory contextual switch manipulation. In the session, rats (n = 8) experienced six consecutive trial blocks, each consisting of ten trials. In block 3, the auditory stimuli originally associated with one of the VR environments (e.g., City) were given in the other VR environment (e.g., Forest), and vice versa in block 4 to create incongruence between visual and auditory contexts. Afterwards (blocks 5 and 6), the original conditions were restored. (B): For each place cell (CA1: n = 103; CA3: n = 35), three separate rate maps were constructed, one based on visual-auditory congruent trials (*blue*) and two (*red*) based on incongruent trials. In the incongruent trials, one (*upper*) was constructed to match the visual contexts of the VR

environments (*vis. match*), and the other (*lower*) was constructed to match the switched, auditory contexts (*aud. match*). Pearson's correlation coefficients between place fields from congruent and visually matched incongruent conditions (or auditorily matched incongruent conditions) were then calculated. Circled numbers indicate block numbers.

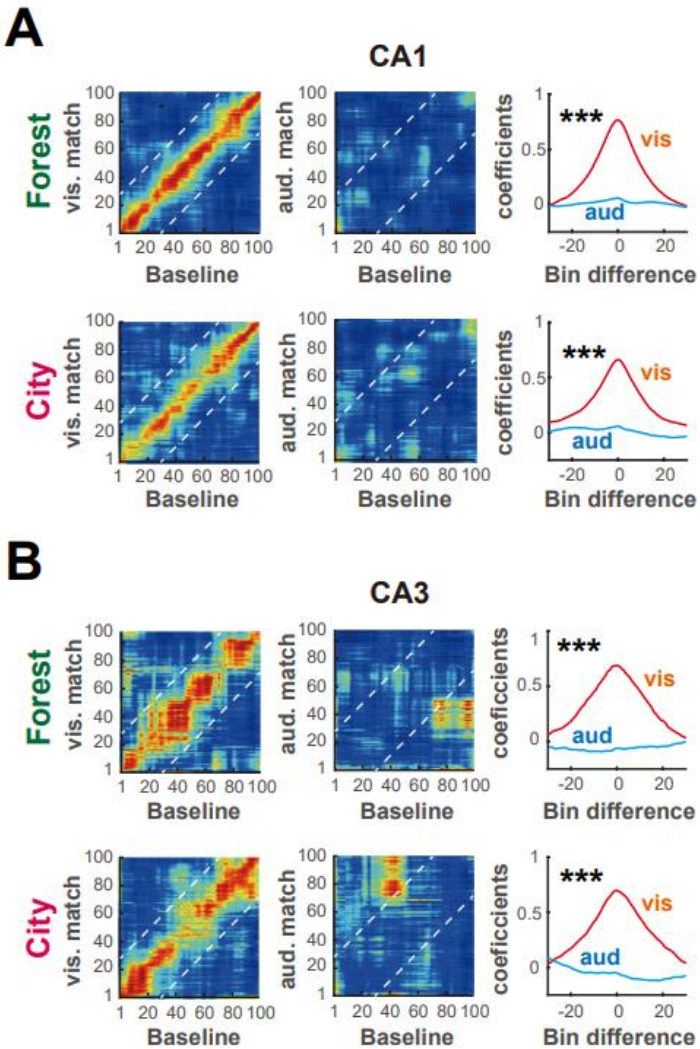

Figure 10. Population vector correlation matrix (PVM) and its linearized graphs from the CA1 (A) or CA3 (B). (*Left*): PVM for the visually matched condition. (*Middle*): PVM for the auditorily matched condition. (*Right*): Quantification of the widths of main diagonal bands determined by averaging correlation values along each diagonal line. Hippocampal cells from a given location showed a significantly higher correlation within the same visual environments compared with the auditory contexts (***$p < 0.0001$; rank-sum test).

The CA1 subregion recruited more place cells in each enriched VR environment than the CA3 subregion specifically, ~44% of the cells recorded from CA1 exhibited place fields at least in one of the environments, whereas only ~33% cells in CA3 ($\chi^2_{(1)} = 24.11$, $p < 0.0001$; Chi-squared test) (**Figure 11**). As shown in prior studies (Leutgeb et al., 2007; Mizuseki et al., 2012), place fields were observed significantly more in CA1 (43.6%, n = 251/576) than in CA3 (33.2%; n = 181/546) ($\chi^2_{(1)} = 21.69$, $p = 0.0003$; Chi-squared test). Overall, the proportion of hippocampal neurons with place fields was equivalent to those reported in the previous VR studies (Aronov and Tank, 2014; Ravassard et al., 2013). Also, CA3 place cells showed a preference for firing in only one of the environments, unlike CA1 place cells. As a result, the proportion of place cells that fired in both environments in CA3 was approximately half of that in CA1 ($\chi^2_{(1)} = 22.82$, $p < 0.0001$; Chi-squared test; **Figure 11**).

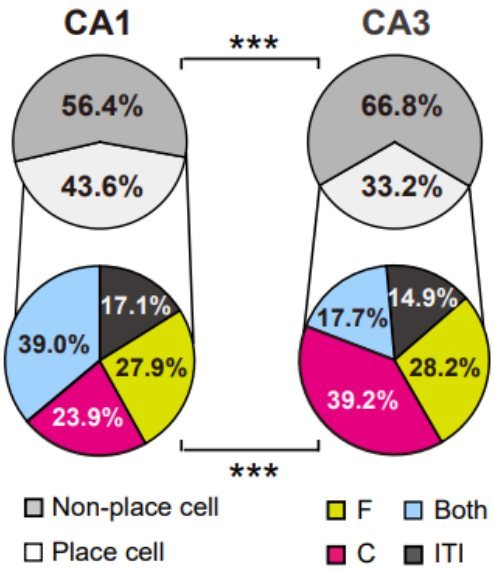

Figure 11. The proportion of place cells from CA1 and CA3 in the virtual environments. F: Forest, C: City, Both: Forest and City, ITI: intertrial interval in the tunnel. ***$p < 0.001$.

For each place cell, I calculated several firing properties: (a) the spatial information score in bits per spike, (b) averaged firing rate, (c) numbers of the place fields, and (d) sparsity per each environmental condition. If the place fields were formed in both environments, basic properties for both environments were computed. These basic firing properties hardly differentiated the two subregions, including spatial information (Forest, Z = -1.54, p = 0.1228; City, Z = 0.82, p = 0.4111; Wilcoxon rank-sum test), average firing rate (Forest, Z = -1.28, p = 0.2009; City, Z = -1.13, p = 0.25), and sparsity (Forest, Z = 0.39, p = 0.6994; City, Z = 1.14, p = 0.25) (**Figures 12**).

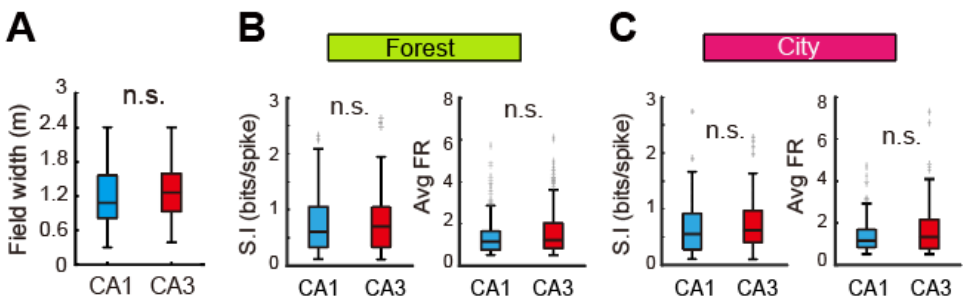

Figure 12. The basic firing properties in the visual enriched virtual environments. (A): Comparison of field width between CA1 and CA3 subregions. (B-C): Comparison of the firing properties (i.e., spatial information score, averaged firing rates) of place cells from CA1 or CA3 within the (B) Forest or (C) City environment. Firing properties were similar in both subregions in each environment.

At the population level, place cells in both CA1 and CA3 represented the entire track in both Forest and City, including the tunnel between the environments (**Figure 13A**). An examination of the population rate maps for the two environments suggested a higher contrast in the spatial firing patterns of place cells between City and Forest (i.e., more regions with darker blue colors for VR areas outside the place cell's receptive field) in CA3 than in CA1. This was confirmed by measuring the environment-specific firing rate-modulation index (RMI), which showed that place cells in CA3 fired more selectively for one of the environments than those in CA1 (p = 0.0001; two-sample Kolmogorov-Smirnov test) (**Figure 13B**). These results are in the same line with the previous studies reporting the higher orthogonality in the CA3 than CA1 (Leutgeb et al., 2007; Leutgeb et al., 2005b; Mizuseki et al., 2012).

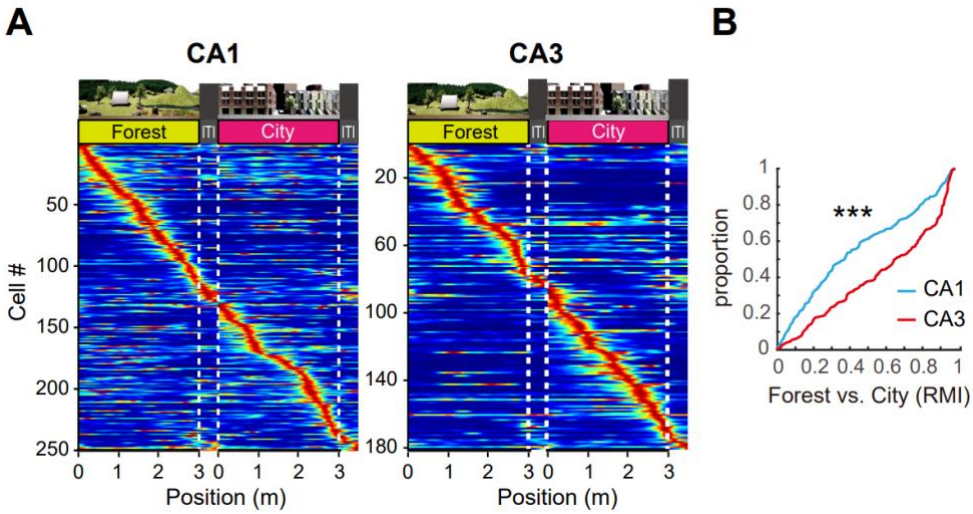

Figure 13. Population rate maps from CA1 and CA3. (A): The rate maps were normalized by their peak firing rates within each cell. The place cells in the CA1 (n = 251) or CA3 (n = 181) uniformly covered each virtual environment. (B): Orthogonal representation of different environments, measured as the rate modulation index (RMI). ***$p < 0.001$.

Lastly, since place fields are recorded without any task demand nor the fixed reward location, I reasoned the place fields to be formed uniformly on the environment rather than to be over-represented in the specific location (Bourboulou et al., 2019; Hollup et al., 2001; Lee et al., 2006) unless there is unexpected salient stimulus on the area. To verify whether place fields all equally formed within each environmental location, I quantified field distribution over the entire track per each environment from CA1 and CA3. Then, I generated the uniform distribution and compared it with each center-of-mass (COM) distribution (**Figure 14**). As a result, there were no differences between COM distribution of CA1 (p = 0.2086, Kolmogorov-Smirnov test) or CA3 (p = 0.1535, Kolmogorov-Smirnov test) from the uniform distribution. In addition, I found no significant difference in the field COM distribution between CA1 and CA3 (p = 0.3851, Two-sample Kolmogorov-Smirnov test; **Figure 14**). These results suggest that fields were formed as a uniform distribution over the entire track. To summarize, these data confirm that our virtual reality system efficiently recruited the place cells to discharge in an environmental-specific manner.

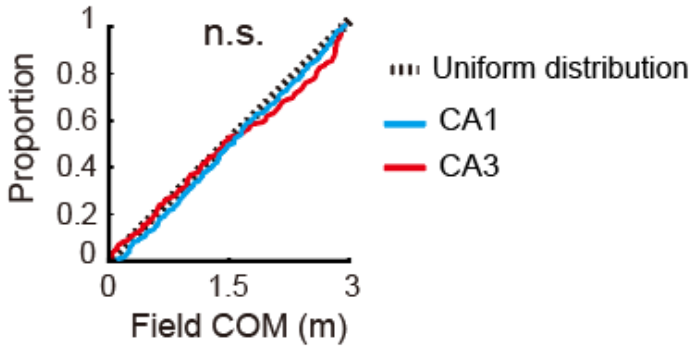

Figure 14. Distribution of Center-of-mass (COM) of the place field CA1 and CA3. There were no differences between the COM distribution of CA1 or CA3 from the uniform distribution, indicating that the place fields all equally represented the virtual environments.

Animals are familiarized in the virtual environments

To verify whether there is any familiarization effect of the animals with the virtual environments, I quantified the number of pauses made by a rat during navigation as an indicator of the degree of familiarization (i.e., training) with the environment. Instantaneous velocity under 0.1 cm/s was used as the criterion for a pause on the track. The proportion of pauses was calculated for each environment from the session by dividing the total paused time by the session duration. For this calculation, I restricted the analysis to the environmental track and excluded the inter-trial interval period (i.e., tunnel). I observed that the number of pauses tended to decrease across sessions ($\chi^2_{(3)} = 6.09$, $p = 0.079$; Kruskal-Wallis test), with the steepest decreasing slope observed between session 1 and session 2 (**Figure 15**). Together, the above-described results indicate that the rats were sufficiently familiarized with the virtual environments (Cushman et al., 2013; Harvey et al., 2009; Youngstrom and Strowbridge, 2012).

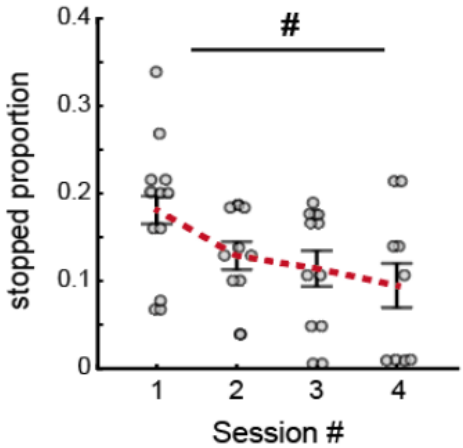

Figure 15. The proportion of pauses during the navigation. Each dot indicates the session within the same environment, and the proportion of pauses displayed a tendency to decrease as the rat experienced more sessions.

Discussion

The VR system has been widely tested for humans and nonhuman primates (Ekstrom et al., 2003; Gulli et al., 2020; Lee et al., 2016; Wirth et al., 2017), but it was not a usual case for rodents. Once the first rodent system had proved that the rats could navigate in the VR environment (Holscher et al., 2005), more VR systems for rodents bloomed in the last decades (Acharya et al., 2016; Aronov and Tank, 2014; Bourboulou et al., 2019; Chen et al., 2013; Dong et al., 2021; Plitt and Giocomo, 2021; Priestley et al., 2022; Radvansky et al., 2021). In a typical rodent VR environment, the animals run on a platform (e.g., styrofoam ball or treadmill) while the head or body is fixed at the center of the platform (Harvey et al., 2009; Holscher et al., 2005). The movement of the platform by the rat induces a matching movement in the visual scenes in the VR environment, usually projected onto surrounding screens or monitors. The rodent virtual reality (VR) system has the enormous advantage of removing intermingled sensory inputs other than visual stimuli, such as tactile and vestibular inputs, allowing the sophisticated examination of behavior and neural networks according to visual stimuli. Thus, during navigation in the VR environment, egocentric spatial information such as vestibular information and path-integrative signal (Chen et al., 2013; Chen et al., 2019; Saleem et al., 2018) must be relatively weak compared to the real world (Ravassard et al., 2013).

Taking advantage of the VR system, I observed the neural activity

of CA1 and CA3 from the head-fixed rats running in virtual environments. In the virtual environments where complex yet rich visual landmarks and backgrounds were composited, I confirmed that the visual scene had a significant influence on the activity of place cells. Also, as previously reported (Leutgeb et al., 2007; Leutgeb et al., 2005b; Mizuseki et al., 2012), I observed more orthogonally tuned place fields across two different virtual environments in CA3 than in CA1. The recurrent collateral is an anatomical feature of CA3 that directly connects among CA3 pyramidal neurons and stores the synaptic strength to represent memory (Bains et al., 1999; Debanne et al., 1998). Due to the connection of recurrent collateral, partial activation of stored representation in CA3 leads to retrieval of the entire representation, called pattern completion (O'Reilly and McClelland, 1994; Rolls, 2013; Treves and Rolls, 1992).

Therefore, by this mechanism, CA3 is characterized by a non-linear response to the stimulus change. Previous studies provide empirical support for this model (Lee et al., 2004; Neunuebel and Knierim, 2014; Vazdarjanova and Guzowski, 2004). When there was a mismatch between local and distal cues in a circular track, neurons in CA3 preserved coherence representation resisting environmental change (Lee et al., 2004). In another study, rats were exposed to two similar environments that differed in their identity or configuration of cues. Immediate early gene expression revealed that CA3 showed a large overlap between populations activated in these two environments neglecting the cue change (Vazdarjanova and Guzowski,

2004). This non-linearity nature of the CA3 well explains the more enhanced yet spatially more tuned recruitment of the CA3 place cell in the virtual environments.

Up to date, numerous results have demonstrated the visually elicited place cells fire in specific locations in the virtual environment (Aronov and Tank, 2014; Chen et al., 2013; Plitt and Giocomo, 2021; Ravassard et al., 2013; Saleem et al., 2018). The dominant influence of visual stimulus in the VR system makes it possible to examine the scene processing of the hippocampal neurons in a more elegant yet controlled fashion.

Chapter 2. The functional role of the CA1 and CA3 in processing the visually modified environment

Introduction

The computational processes of the hippocampal networks have been studied with ambiguous inputs created using two major methods: One is to remove some of the cues in the original environment to provide partial inputs, and the other is to degrade the original inputs by adding noise (O'Reilly and McClelland, 1994). The processing of noisy input patterns has been considered a key test in computational modeling to diagnose the performance of an attractor network (e.g., a Hopfield network), such as that presumably residing in the CA3 subregion of the hippocampus (Churchland and Sejnowski, 1992; Treves and Rolls, 1994). However, despite the theoretical importance of testing a network's behavior with noisy input patterns, it has proven almost impossible to create an experimental condition allowing researchers to add parametrically quantifiable noise to the environment in real experimental settings. Therefore, research on pattern completion in the hippocampus has largely focused on providing partial cues by removing some of those present in the original environment (Jo et al., 2007; Nakazawa et al., 2002; Zorzo et al., 2021).

In this study, I used a VR experimental setup to parametrically introduce sensory noise to the original environment to controllably test the hippocampal networks. Having established the VR conditions in which place cells in both CA1 and CA3 were robustly and differentially recruited across the two virtual environments (**Chapter 1**), I further examined the

neural responses of the CA1 and CA3 by adding visual noise (i.e., virtual fog) into the familiar environments.

Materials and methods

The experimental settings for the fog manipulation session

A virtual foggy environment was created by adding a visual fog effect to the familiar Forest or City environment (fog session). To parametrically manipulate the amount of visual noise (i.e., 0%, 15%, or 30% fog), I calculated a structural similarity index (SSIM) between the original and foggy environments (Rikhye and Sur, 2015; Wang et al., 2004) (**Figure 16**). SSIM is an image quality metric that comprehensively reflects an image's characteristics based on its luminance, contrast, and structure criteria (Wang et al., 2004; Yu et al., 2018). I simulated 'virtual fog' by applying the 'Exponential Height Fog' function provided by *Unreal Engine 4*. This function allowed the creation of fog effects based on the falloff and height parameters. Once I adjusted the falloff parameter to produce global fog effects on the virtual environments, the density of fog was manipulated by adjusting the height parameter. Only one of the environments was used for the fog-manipulation recording session, which lasted for 4 days, and Forest and City environments were equally presented in a counterbalanced manner. For each session, approximately 18 trials were performed as a baseline at the beginning of the session. Afterward, three different fog conditions (i.e., 0%, 15%, 30% fog conditions; 18 trials/condition) were pseudo-randomly presented throughout the session.

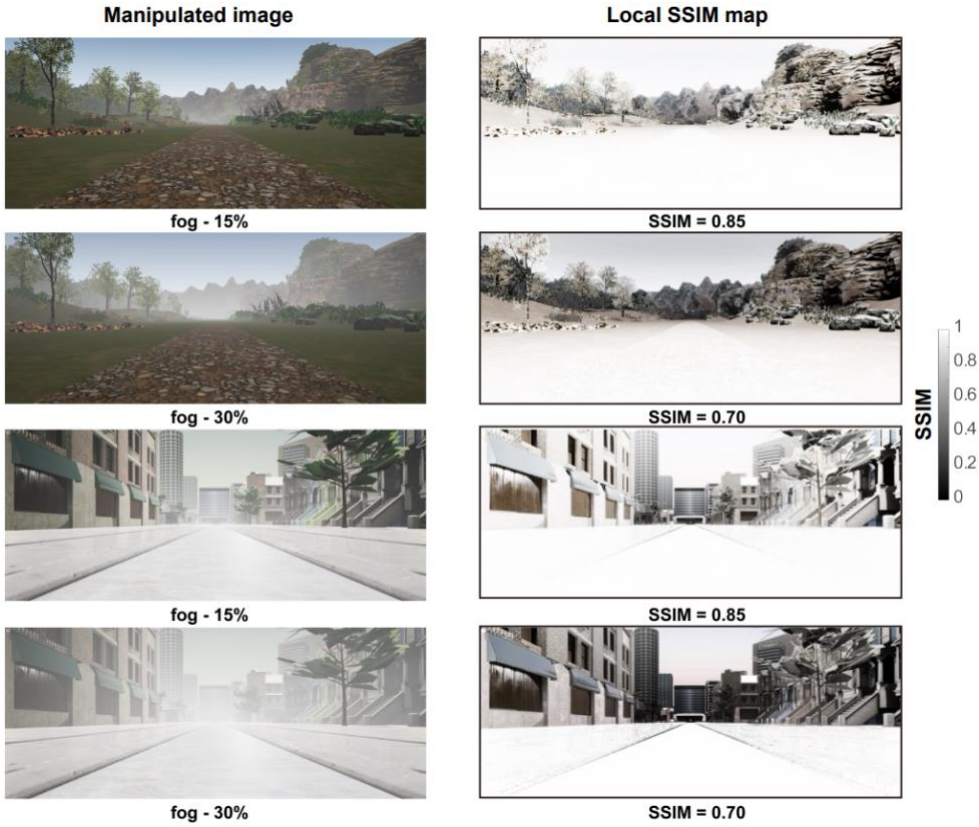

Figure 16. Adding visual noise to the environments. The physical similarities between the original and foggy environments were calculated by the structural similarity index measure (*SSIM*). Using this metric, I chose three noise levels to alter the original environment: fog 0%, identical to the original image; fog 15%; and fog 30%. The darker frame area indicates the more visually affected part of the environment.

Detecting pupil dilation

The shape of the eye was extracted by first binarizing raw images with values ranging from 0 to 255 into 0 (black) or 1 (white) by applying a threshold. The threshold was determined for each session by visually analyzing the movie's random frames that best segregated the region of the interest (i.e., eye) from the background. The following morphological image processing steps were then performed: a) small objects under the threshold (< 1000 pixels) were first excluded (i.e., opening), then b) the contours of the remaining objects were smoothed (i.e., closing) to emphasize the eye's contours. The pupil region was extracted using a circle-fitting algorithm that detects the pupil's mean [x, y] coordinates from the binarized image. The number of pixels under the designated pupil area was counted and used as the pupil size for analysis. Pupil sizes were Z-scored for each session before further analyses.

Population vector correlation analysis

I constructed an autocorrelation matrix for each cell (Gothard et al., 1996; Lee et al., 2004) to quantify the cell's spatial representation at the neural population level. A population rate map composed of the individual rate maps (each normalized by the cell's maximum firing rate) was defined as follows:

$$P_i^c = \frac{\lambda_i^c}{\bar{\lambda}_i}$$

where the index c indicates all cells, and λic is the firing rate for the c th cell at position bin i. Each neuron was normalized by the mean spike rate $\lambda \bar{i}$ to prevent the population vector from being confounded by the cells with the highest firing rates. Next, the correlation between the two vectors from the same population rate map was computed using the following equation for obtaining the Pearson correlation coefficient:

$$r_{ij} = \frac{\sum_{c=1}^{n} (P_i^c - \bar{P}_i)(P_j^c - \bar{P}_j)}{\sqrt{\sum_{c=1}^{n} (P_i^c - \bar{P}_i)^2 (P_j^c - \bar{P}_j)^2}}$$

where i and j denote the population vector composed of the rate maps from each fog condition, n indicates the number of cells, while c indicates c th cell in the population. P is the firing rate of the cell, and $\bar{P}$ is the mean firing rate of the vector. As an output, the symmetric matrix was computed for each condition. Then, the change in the mean correlation coefficients under each condition were statistically compared using the Wilcoxon rank sum test (Neunuebel et al., 2013; Park and Lee, 2016).

Results

Place cells show significantly greater remapping in CA1 than in CA3 upon introduction of subtle visual changes in the familiar VR environment

Having established the VR conditions in which place cells in both CA1 and CA3 were robustly and differentially recruited between the two environments, I compared the neural responses of the two subregions to subtle modifications in the familiar environment by introducing visual noise (i.e., fog) into the Forest or City (**Figure 17**). The degree of physical similarity between the original and foggy environments was calculated as a 'structural similarity index measure' (*SSIM*), an image quality metric that reflects the image's comprehensive characteristics based on its luminance, contrast, and structure criteria (Wang et al., 2004; Yu et al., 2018). Based on the *SSIM* measure, three levels of fog were chosen to add visual noise parametrically to the original environment. After the rat finished 18 trials in one of the familiar environments, I initiated a fog trial block in which different fog conditions were introduced pseudo-randomly (0%, 15%, and 30%; 18 trials per condition; **Figure 17**).

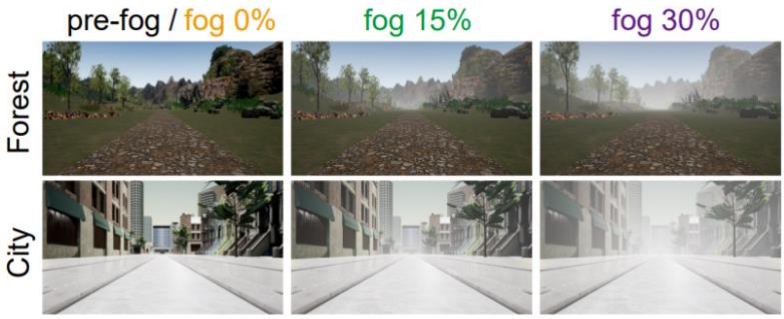

Figure 17. Sample screen-captured scenes taken at the start location of each visually enriched environment under different fog conditions (0%, 15%, and 30%).

To examine changes in spatial firing patterns associated with the fog manipulations, I calculated the correlation coefficient between the rate maps for the pre-fog condition and for each fog condition (0%, 15%, or 30%) for place cells in CA1 (n = 331) and CA3 (n = 160). Place cells that satisfied the following criteria were included in the analysis: (i) mean firing rate > 0.5 Hz in at least in one fog condition during the recording session, (ii) spatial information > 0.1 (bit/s), and (iii) *p*-value of spatial information < 0.001. For each place cell, I obtained the place fields associated with the individual fog conditions (i.e., pre-fog, fog-0%, fog-15%, and fog-30%) (**Figure 18**). At the single-unit level, some place cells in CA1 (cells 588-10-02-04 and 536-10-13-03 in **Figure 19A**) and CA3 (all cells in **Figure 19B**; for more examples, see **Figure 20A and 20B**) maintained their firing fields across different fog conditions. In other cases, a place cell exhibited "global remapping", characterized by a shift in place-field location or appearance/disappearance of a place field (Leutgeb et al., 2005b), as fog was introduced (CA1 cells *511-09-04-08*, *511-09-04-05*, *564-10-09-07*, *477-07-21-01*, *526-08-17-02* in **Figure 19A**; for more examples, see **Figure 20A and 20B**).

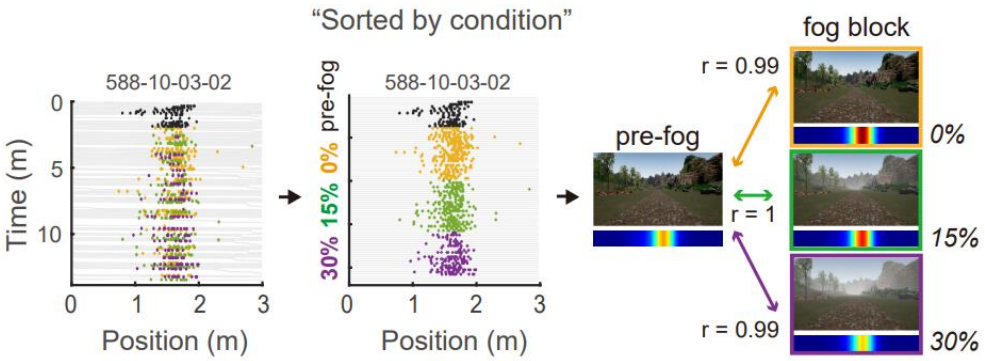

Figure 18. Example of a place cell the fog session. (*Left*): Raw spikes in the VR environment for individual trials. Black dots and colored dots indicate baseline and fog conditions, respectively. Spiking activities from fog-0%, fog-15%, and fog-30% trials are shown in orange, green, and purple, respectively. (*Right*): Rate maps constructed for pre-fog and the three fog conditions. Pearson's correlation coefficients between pre-fog and each fog condition are shown. physical similarities between the original and foggy environments were calculated by the structural similarity index measure (SSIM). Using this metric, I chose three noise levels to alter the original environment: fog 0%, identical to the original image; fog 15%; and fog 30%. The darker frame area indicates the more visually affected part of the environment.

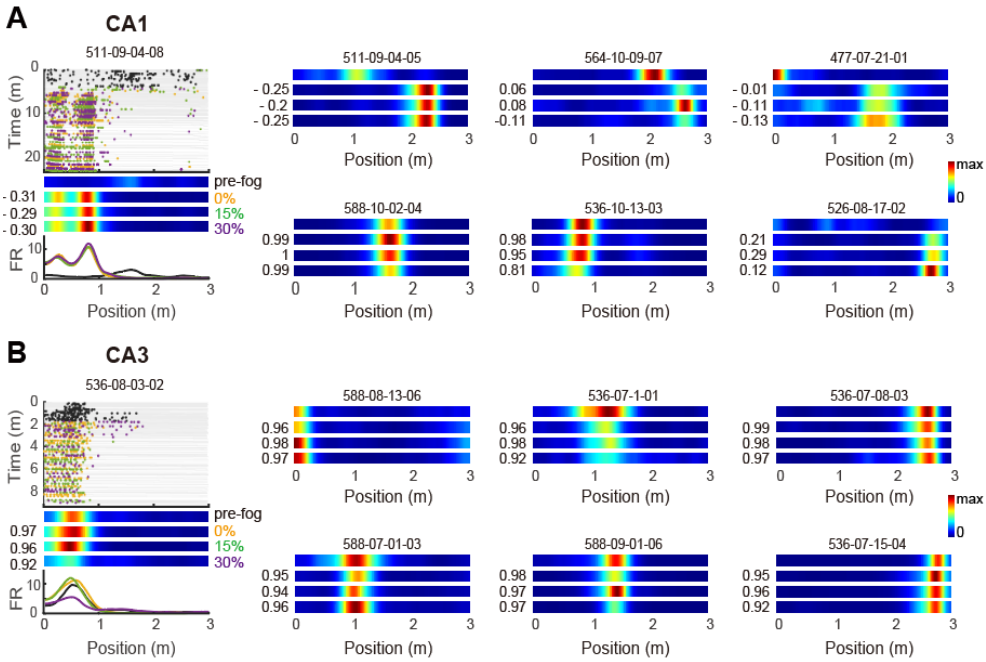

Figure 19. Representative neural firing patterns of single units recorded from CA1 (A) and CA3 (B). (A): A subpopulation of CA1 cells maintained their spatial firing patterns (*588-10-02-04*; *536-10-13-03*) while others showed global remapping (*511-09-04-08*; *511-09-04-05*; *564-10-09-07*; *477-07-21-01*; *526-08-17-02*) across the fog conditions. (B): In contrast, relatively coherent spatial firing patterns were observed in CA3 (*536-08-03-02*; *588-08-13-06*; *536-07-1-01*; *536-07-08-03*; *588-07-01-03*; *588-09-01-06*; *536-07-15-04*).

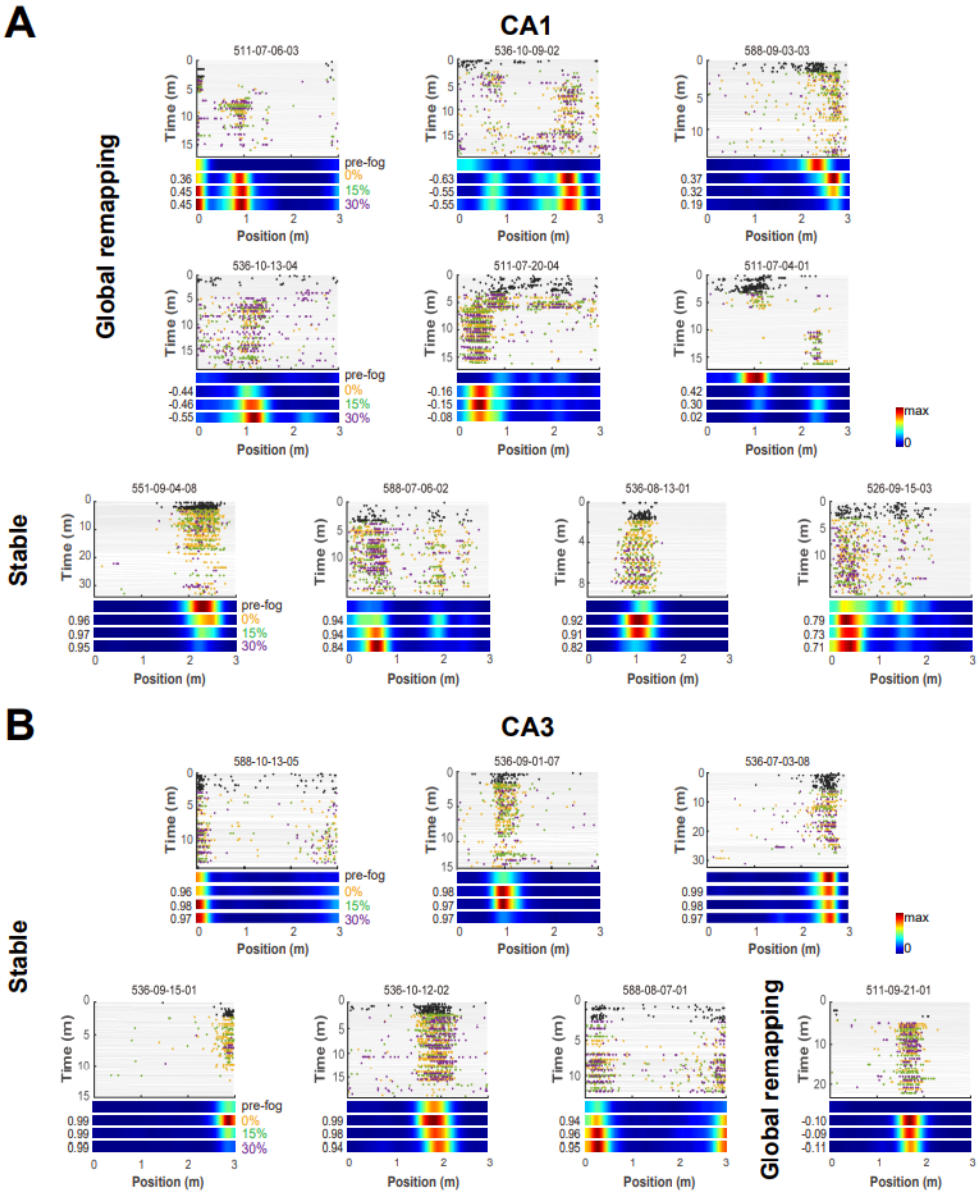

Figure 20. More examples of the place cells in CA1 (A) and CA3 (B) subregions in the fog manipulation session.

Overall, rate map similarities for place cells (measured as spatial correlation) compared with pre-fog conditions were significantly lower in CA1 than in CA3 for each of the fog-manipulated conditions. A two-way ANOVA revealed main effects of the fog condition ($F_{(2, 1467)} = 7.36$, $p = 0.0007$) and subregion ($F_{(1, 1467)} = 78.34$, $p < 0.0001$), but showed no interaction between the two factors ($F_{(2, 1467)} = 0.02$, $p = 0.983$) (**Figure 21)**. In addition, the rate-map similarities were significantly greater when the different fog conditions were compared with the pre-fog condition, compared to when the different fog conditions were compared with each other within the fog block ($p < 0.0001$; two-sample Kolmogorov-Smirnov test) (**Figure 22**), and this contrast was greater in CA1 than in CA3 (**Figure 21**).

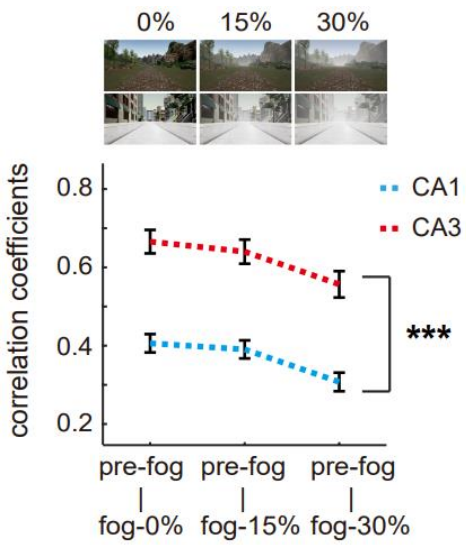

Figure 21. Correlation coefficients between rate maps for pre-fog and each fog condition for CA1 and CA3 cells. The correlation coefficients were calculated from pre-fog vs. fog conditions within each cell. Then,

averaged correlation coefficients were stacked in the same graph to examine if there were any quantitative differences across the subregions. Significantly lower coefficients were observed in the CA1 (n = 331) than in CA3 (n = 160) (*** $p < 0.001$). Error bars indicate SEM.

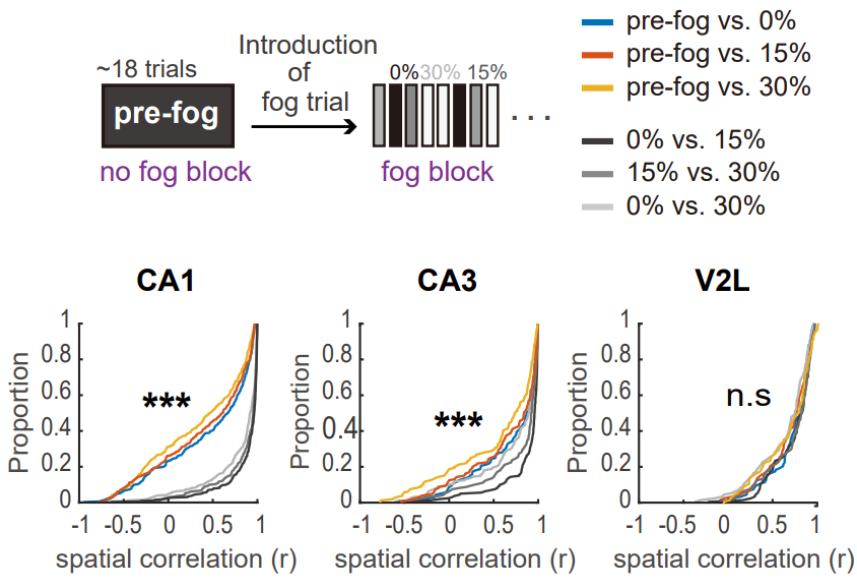

Figure 22. The cumulative distribution of spatial correlation for each comparison. Spatial representations were significantly consistent within the fog block in both CA1 and CA3 ([pre-fog vs. fog-0%; pre-fog vs. fog-15%; pre-fog vs. fog-30%] vs. [fog-0% vs. fog-15%; fog-0% vs. fog-30%; fog-15% vs. fog-30%]: $p < 0.0001$; two-sample Kolmogorov-Smirnov test). In contrast, cells in V2L did not differentiate the contextual change between the pre-fog and fog blocks ($p = 0.1175$; two-sample Kolmogorov-Smirnov test).

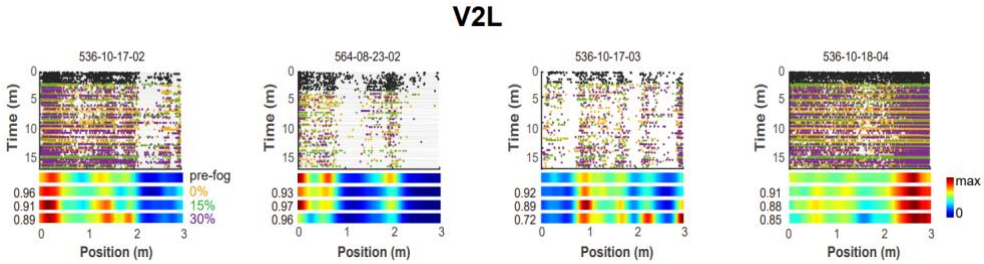

Figure 23. Representative neural firing patterns of single units recorded from the visual cortex (lateral extrastriate visual cortex; V2L). Examples of location-sensitive cells in V2L.

Compared to the firing patterns of place cells in the hippocampus, cells recorded in the visual cortex (n = 101) in the same rats exhibited coherent firing patterns across the fog conditions (**Figure 23**), and thus did not reflect the contextual change between the fog conditions (p = 0.1175; two-sample Kolmogorov-Smirnov test) (**Figure 22**). It is unlikely that the remapping reported here was caused by a temporal drift or artifact during recording, as I verified that the waveforms of the majority of single units were similar for sleep sessions recorded before and after the VR recording session (**Figure 24**).

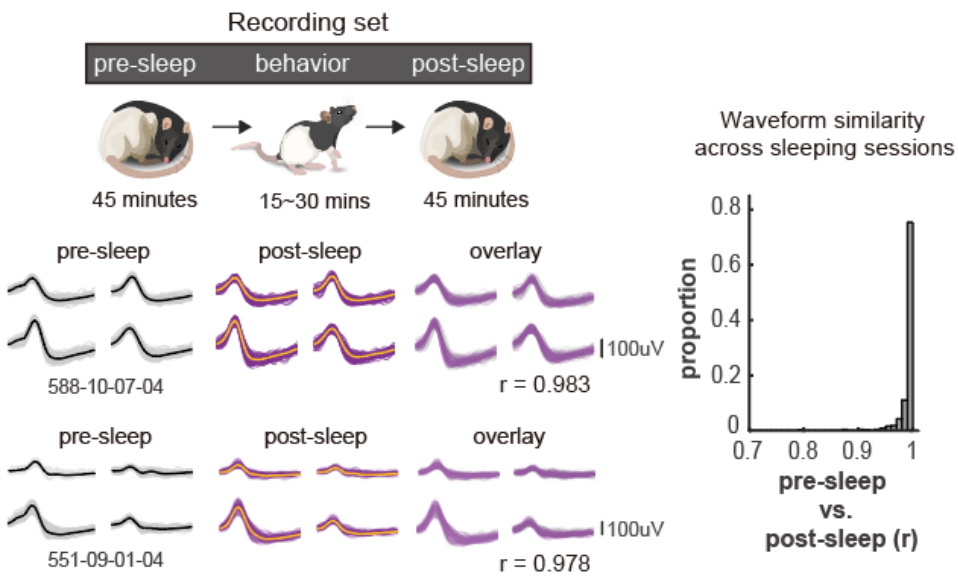

Figure 24. The spike waveforms of a single unit before and after the recording session. Waveform similarity was measured by calculating Pearson's correlation between the averaged waveforms from the pre-sleep and post-sleep sessions. I confirmed that most of the single units used for the analysis showed high similarity (r > 0.9) across the sleep sessions.

To further test the significance of the change in spatial firing patterns between pre-fog and fog block epochs, I generated surrogate rate maps by shifting the timestamps for spike trains forward or backward in random increments. Then, I calculated Pearson's correlation using each surrogate rate map. I repeated this process 1000 times to obtain the distribution of correlation values. I defined a stable cell as one in which the spatial correlation coefficient between pre-fog and fog-0% rate maps passed a significance threshold of $p < 0.05$ from the bootstrapped distribution (yellow bars in **Figure 25A**). Place cells that did not pass the significance threshold were defined as undergoing global remapping (blue bars in **Figure 25A**). I found that more cells remapped globally in CA1 than in CA3 ($\chi^2_{(1)} = 20.49$, $p < 0.0001$; Chi-square test) (**Figure 25B**). Global remapping cells were distributed throughout the dorsal CA1, and I did not find any anatomical clustering in a particular region (**Figure 26**).

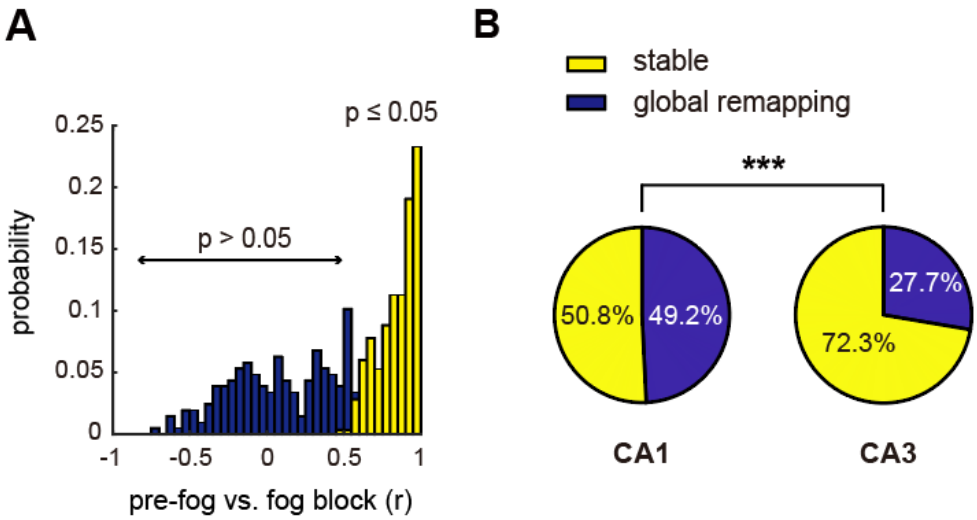

Figure 25. Proportions of stable versus global remapping cells in CA1 and CA3. (A): Distribution of correlation coefficients calculated between pre-fog and fog block rate maps. Yellow bars indicate "stable cells", defined as those with a spatial correlation coefficient between pre-fog and fog-0% rate maps that passed a significance threshold of $p < 0.05$ from the bootstrapped distribution. Blue bars indicate "global remapping cells." (B): The pie graph of classified cell types from CA1, CA3. The proportion of either stable or global remapping cells was visualized as the pie graph for each region. The proportion of cells with global remapping were significantly higher in the CA1 than CA3 (*** $p < 0.0001$).

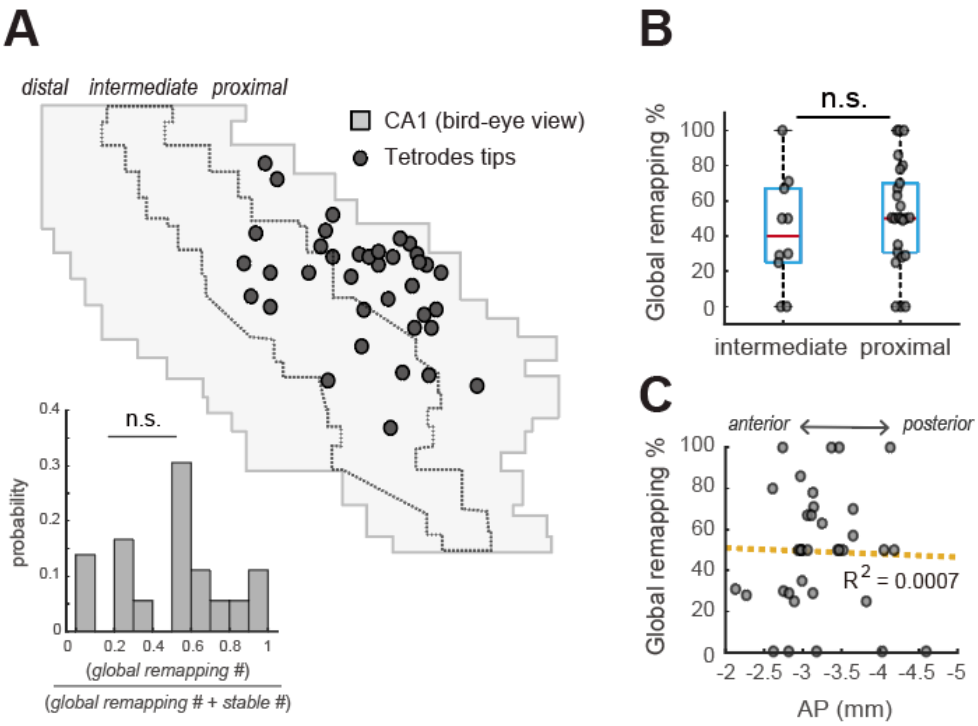

Figure 26. The Proportions of stable versus global remapping cells in CA1 along with the sampling location. (A): Electrode tips were verified with histology and visualized along the proximo-distal and anteroposterior axes in CA1. I constructed a flat map using coronal brain sections of all animals. Nissl-stained sections were aligned to vertically orient the tetrode tracks, and the length of the CA1 layer was measured using the *ImageJ* software. Due to individual differences in brain sizes and sectioning angles, I adjusted the flat maps proportionally for all rats by referencing the medial habenular nucleus and superior colliculus. I then marked the relative tetrode tip positions on the flat map as dots. To define the intermediate-proximal border, I divided the proximo-distal axis into three divisions evenly

(Deshmukh, 2021; Henriksen et al., 2010). If the global remapping and stable place cells were differentially distributed along the superficial-deep axis in the principal cell layer of CA1, I expected that a particular type of place cells (global remapping or stable) would be more frequently observed by particular tetrodes (presumably recording from either the superficial or deep layer). If that was the case, then one would expect the distribution of the proportions of place cells undergoing global remapping to exhibit a bimodal distribution. However, the distribution of the proportion of global remapping cells (the number of global remapping cell divided by the sum of the numbers of global remapping and stable cells) showed a uniform distribution ($\chi^2_{(1)} = 2.78$, $p = 0.0956$, Chi-square goodness-of-fit test with uniform distribution) (B-C): Percent global remapping scores were compared by intermediate vs. proximal (B), anterior vs. posterior (C) axis. I found no significant difference along the proximo-distal axis ($\chi^2_{(1)} = 2.31$, $p = 0.13$; Chi-squared test) and nonsignificant trends ($R^2 = 0.0007$) across the anteroposterior axis.

Interestingly, when a place cell remapped globally as the rat started experiencing the fog block, it also remapped in the fog-0% condition (see CA1 cells *511-09-04-05*, *511-09-04-08*, *477-07-21-01*, *526-08-17-2* in **Figure 19A**). Because fog-0% was physically identical to the pre-fog condition, it is possible that global remapping in fog-0% could be induced by a top-down signal. In support of this possibility, I confirmed that the rat's pupil dilation responded to the amount of change during manipulation, including the pre-fog to fog-0% change (**Figure 27**).

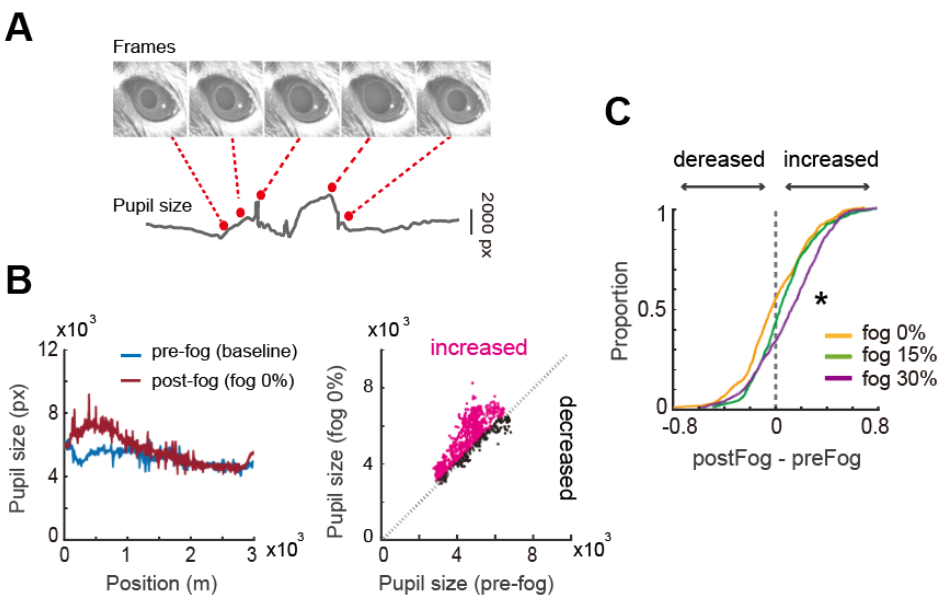

Figure 27. Adding visual noise to a familiar environment affected attention level of animals. (A): Extracted pupil size data. (B): Representative pupillometry data from an individual session. Left: Averaged pupil size for each location for pre-fog (*blue*) and fog-0% (*red*) conditions. Right: Pupil sizes for pre-fog and fog-0% conditions paired to the same

positions of the environment. Pairs with increased pupil sizes in fog-0% are shown in magenta. (C) The proportion of increased or decreased pupil sizes plotted as cumulative distributions across fog conditions. As fog became denser, the pupil size increased significantly compared with the pre-fog condition at the same locations ($\chi^2_{(2)} = 6.95$, $p = 0.0309$; Kruskal-Wallis test).

Next, I measured whether the amount of remapping in the fog-0% condition changed across trials within a session as the rat experienced more fog conditions (fog-15% and fog-30%) as trials proceeded (**Figure 28**).

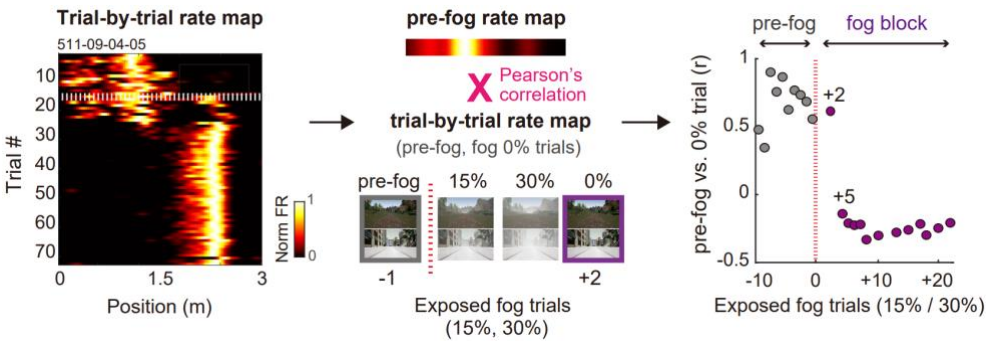

Figure 28. Temporal neural dynamics of the place cell in the fog session. Example cell in a fog manipulation session. (*Left*): Stacked individual rate maps for all trials. The white dotted horizontal line indicates the trial from which the fog block started. (*Middle*): Pearson's correlation coefficient computed between the rate maps of the pre-fog block and fog-0% trial in the fog block. (*Right*): Correlation coefficients for all fog-0% trials plotted as a function of the number of fog trials (fog-15% and fog-30% combined) experienced before the fog-0% trial of interest. Global remapping was not evident when the rat experienced two fog trials (+2), but was clearly visible after experiencing five fog trials (+5).

I found that, on average, global remapping in fog-0% occurred almost immediately after the fog block started, and the amount of remapping abruptly increased after the rat experienced a few trials of the fog condition (Z = 2.49, p = 0.0127; Wilcoxon rank-sum test) (**Figure 29A**). Furthermore, the firing rate of place cells increased gradually in fog-0% trials as the rat experienced more fog trials (Z = -4.03, p < 0.0001; Wilcoxon rank-sum test) (**Figure 29B**). There was also a learning effect across days in place cells that underwent global remapping in CA1 but not in stable cells (**Figure 30**).

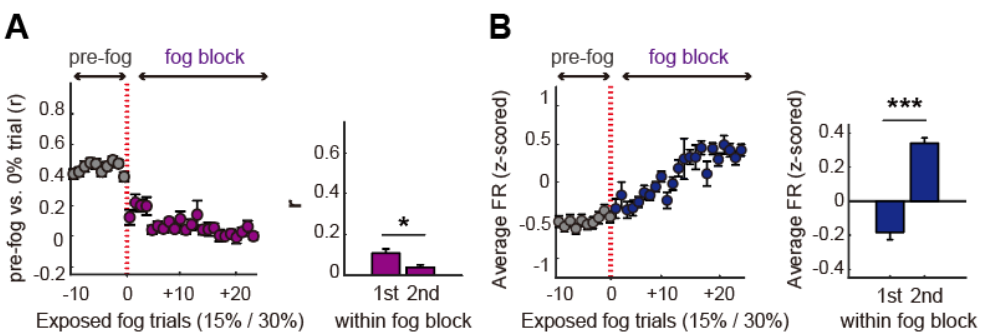

Figure 29. Abrupt global remapping is followed by a gradual increase of the firing rate in CA1 with the introduction of fog trials. (A): *Left*: Mean correlation coefficients between the averaged rate map for pre-fog and those for individual pre-fog trials (*gray*), and those between the average rate map for pre-fog and individual fog-0% trials (*purple*). Only place cells in CA1 that underwent global remapping were used (n = 163). The abscissa follows the same scheme as in (A). Error bars indicate SEMs. *Right*: Trials grouped into two equal sub-blocks (1st and 2nd half) within the fog block, and the

mean correlation coefficient for each sub-block, presented as a bar plot. *p < 0.05. (B): *Left*: Mean firing rates visualized with the same scheme as in (B) for all place cells that underwent global remapping in CA1. *Right*: Mean firing rates for first and second halves compared with each other. Error bars indicate SEMs. ***p < 0.001.

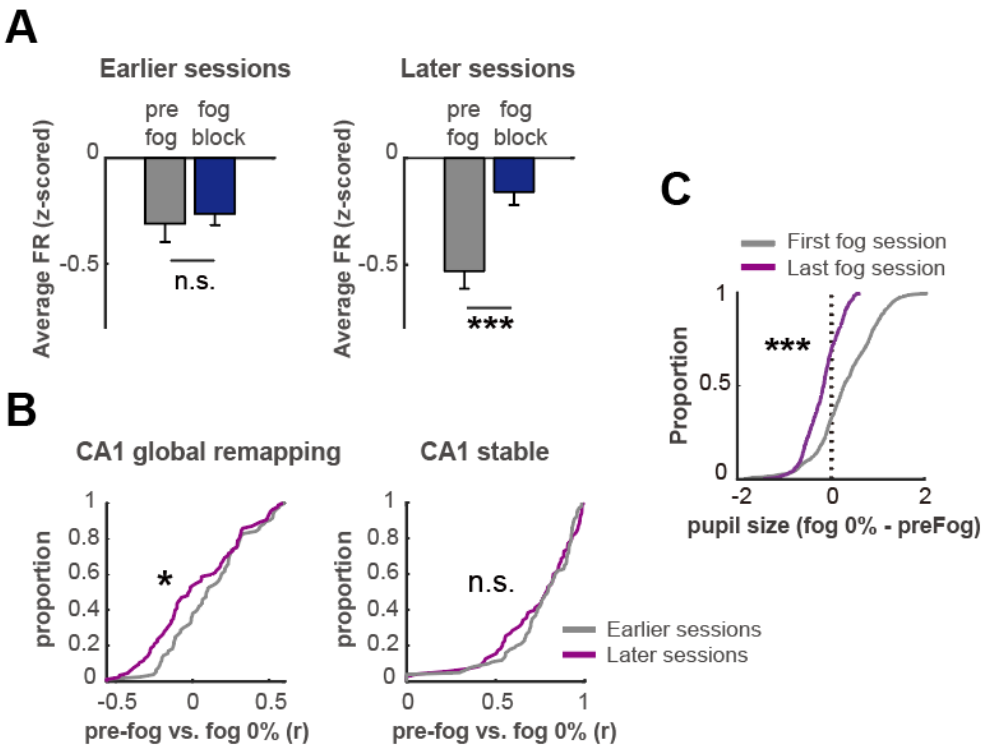

Figure 30. Global remapping cells in CA1 is shaped by fog experiences. (A): Normalized mean firing rates from the last 8 consecutive trials in the pre-fog block and from the first 8 trials for the fog block. Earlier sessions: Day 1 to 2. Later sessions: Day 3 to 4. Global remapping in CA1 was greater in later sessions than in earlier sessions (Earlier sessions, Z = -1.77, p = 0.08; Later sessions, Z = -4.44, p < 0.0001). Error bars indicate SEM.

(B): Cumulative distribution of correlation coefficients calculated between the rate maps of pre-fog and fog blocks. For the CA1 global remapping cells, the global remapping was more readily observed (presumably due to the expectation of ‘fog trials’) in later sessions than in earlier sessions ($Z = 2.02$, $p = 0.04$, Wilcoxon rank-sum test); however, no such difference was found in CA1 stable cells ($Z = 0.44$, $p = 0.66$; Wilcoxon rank-sum test). (C): Differences in pupil size between pre-fog and fog conditions across days. As the rat experienced more fog sessions, pupil size in the fog-0% condition decreased significantly in later sessions ($Z = 4.32$, $p < 0.0001$; Wilcoxon rank-sum test), indicating that the arousal level subsided across sessions.

In CA1, but not in CA3, subtle visual noise evokes heterogeneous subpopulations of place cells undergoing rate and global remapping

I further compared the global remapping cells with stable cells at the population level. I aligned the CA1 place fields in the pre-fog condition according to their firing positions in the virtual track and found that the entire track was covered homogeneously (**Figure 31A-i**). When that order of place cells in the population rate map was carried over to different fog conditions (including fog-0%), the spatially organized patterns of place fields along the diagonal disappeared, as most of the place cells remapped globally (**Figure 31A-i**). Notably, CA1 place cells did not remap randomly across different fog conditions. Instead, once remapped, place cells maintained their field locations across the different fog conditions (including fog-0%) within the fog block (**Figure 31A-ii, iii**). This finding suggests that, in CA1, the subpopulation of global remapping cells may have created a new map dedicated to the fog block. Another subpopulation may represent the original environment, as the place cells in this subpopulation (i.e., stable cells) maintained their firing locations of the pre-fog condition throughout the fog conditions (**Figure 31B-i, ii**). In CA3, in contrast, most place cells were stable cells (**Figure 32-i, ii**). Although the proportions of the global remapping cells varied across animals (**Figure 33A**), the proportion of place cells that underwent global remapping was higher in CA1 than in CA3 for most sessions ($p < 0.0001$; Wilcoxon signed-rank test) (**Figure 33B**).

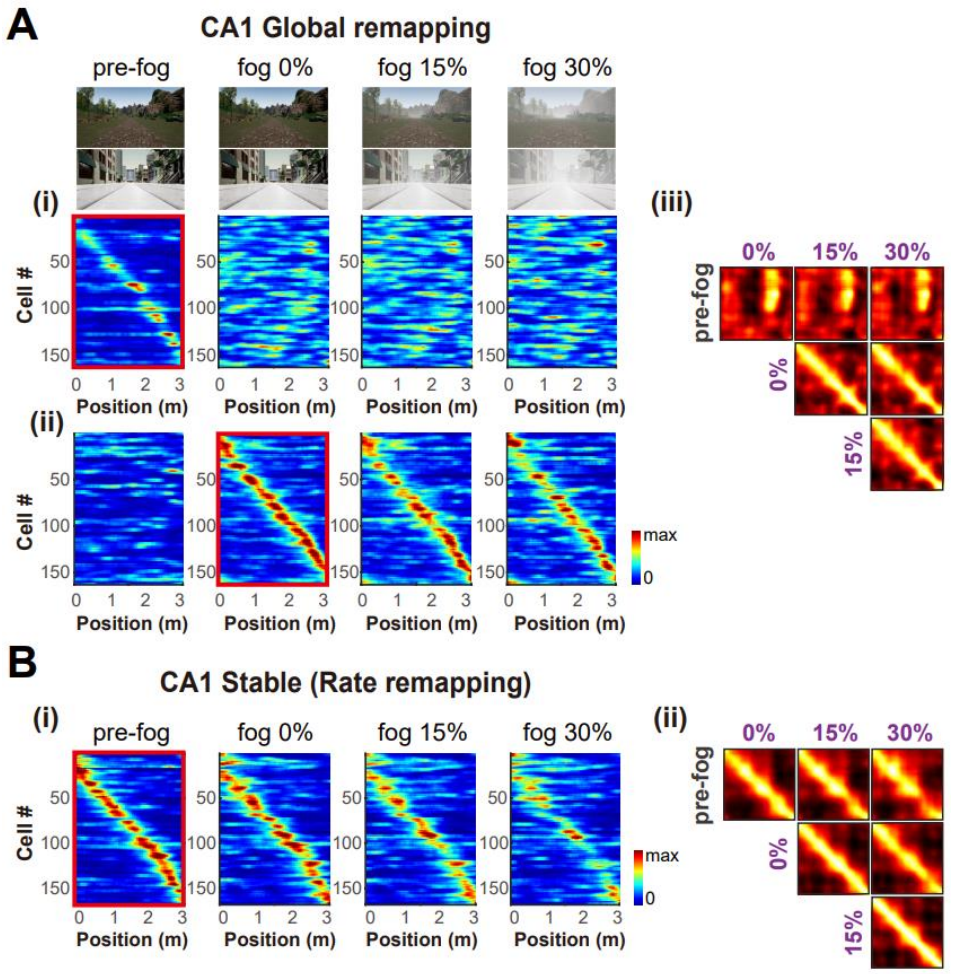

Figure 31. Global remapping and rate remapping subpopulations of place cells in CA1 code distinct types of changes in the environment. (A): Rate maps across fog conditions generated for each place cell. Rate maps were aligned by peak from the pre-fog condition (i) or fog 0% condition (ii), indicated by the red box, in CA1 place cells that underwent global remapping (n = 168). For each subpopulation, a population vector correlation matrix (PVM) was constructed to depict spatial firing patterns across fog conditions (iii). (B): Aligned rate maps and PVMs of stable place cells in CA1.

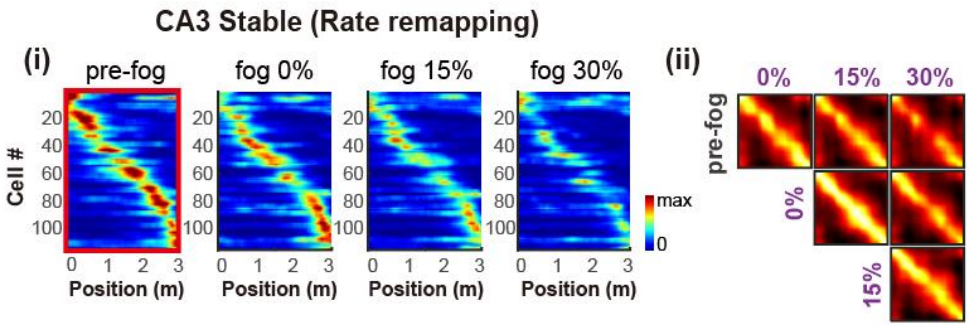

Figure 32. Aligned rate maps and PVMs of stable place cells in CA3. Rate maps across fog conditions generated for each place cell in CA3 (n = 116). Rate maps were aligned by peak from the pre-fog condition (i), indicated by the red box. A population vector correlation matrix (PVM) was constructed to depict spatial firing patterns across fog conditions (ii).

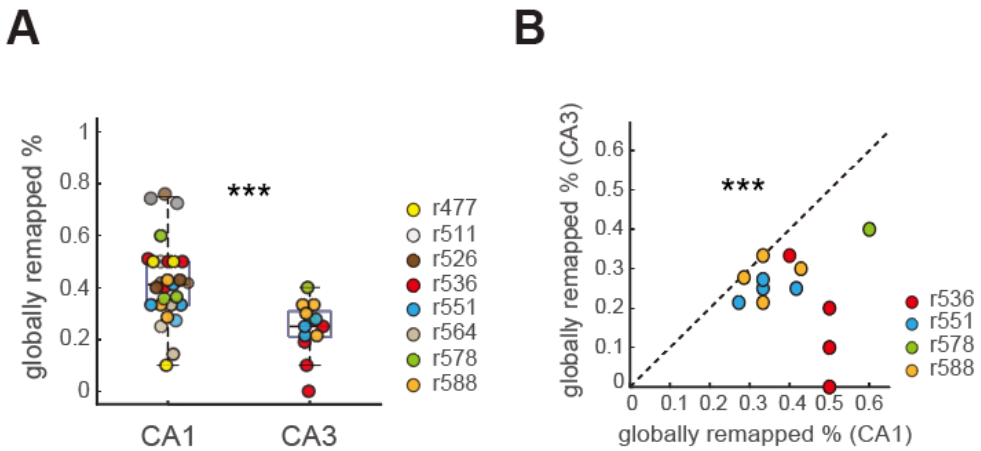

Figure 33. The proportion of the globally remapping cells for each session. (A): Each dot indicates the recording session. I confirmed the presence of more global remapping cells in CA1 than in CA3 across sessions ($p < 0.0001$; Wilcoxon rank-sum test). (B): I extracted the sessions with at least four analyzed place cells from both CA1 and CA3 and directly compared the proportions within the simultaneously recorded session. Global remapping cells were present significantly more in CA1 than in CA3 ($p < 0.0001$; Wilcoxon signed-rank test).

In addition, the differential activity patterns between global remapping and stable cells across different comparative conditions were found in all rats (**Figure 34**).

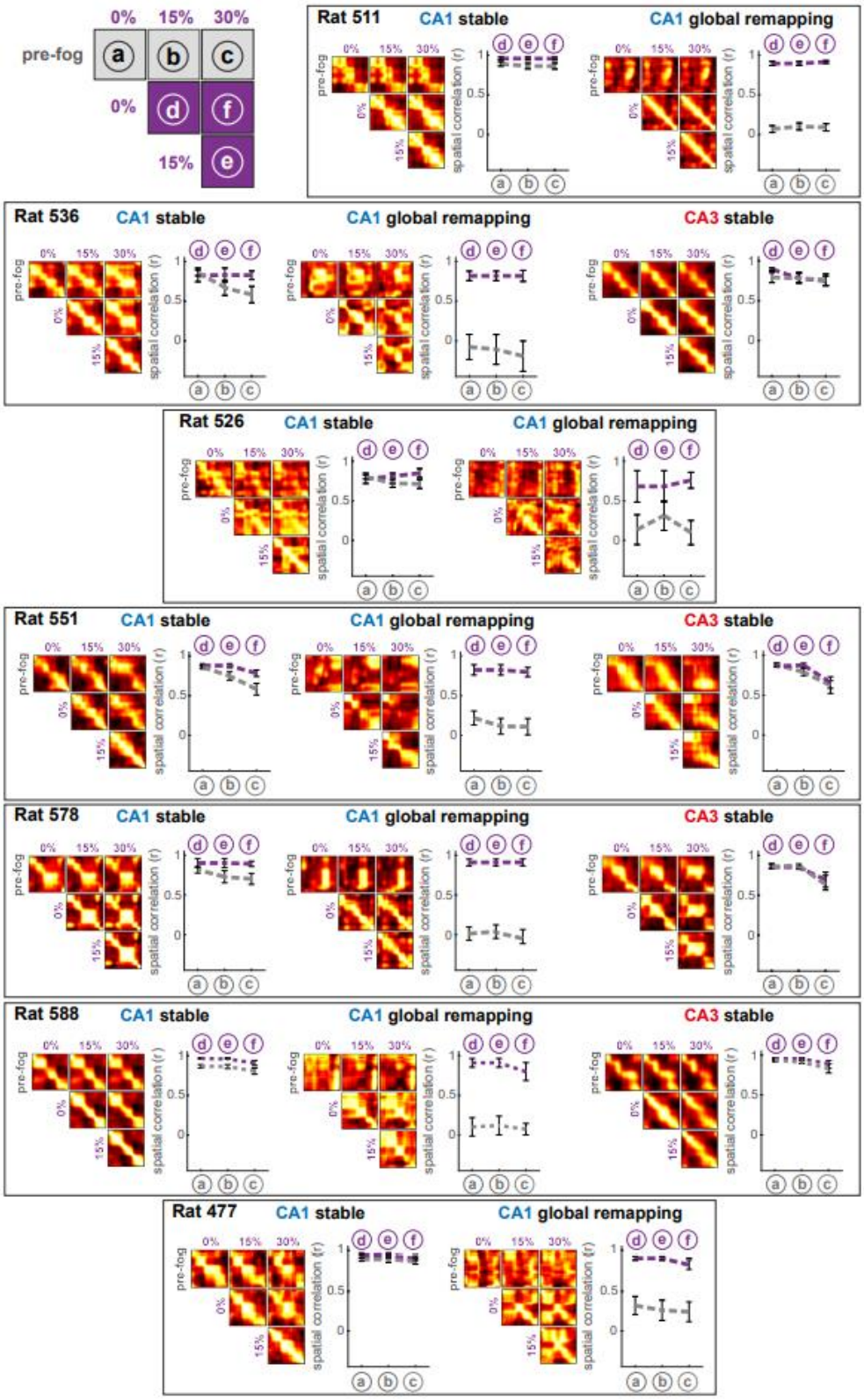
0% 15% 30%
pre-fog
a b c
0%
d f
15%
e
Rat 511
CA1 stable
CA1 global remapping
Rat 536
CA1 stable
CA1 global remapping
CA3 stable
Rat 526
CA1 stable
CA1 global remapping
Rat 551
CA1 stable
CA1 global remapping
CA3 stable
Rat 578
CA1 stable
CA1 global remapping
CA3 stable
Rat 588
CA1 stable
CA1 global remapping
CA3 stable
Rat 477
CA1 stable
CA1 global remapping
spatial correlation (r)

Figure 34. Each remapping type exhibits coherent patterns across the individual animals. For each animal (n = 7), I computed a correlation matrix by calculating the correlation coefficient between two population vectors from the pre-fog condition and each fog condition or from two possible fog conditions to visualize the spatial firing patterns of each subpopulation (*left*). I also calculated mean correlation coefficients for corresponding conditions and visualized each condition as a line graph (*right*). I found that the proportions of global remapping cells varied across individual sessions or animals, but the neuronal types of remapping were preserved across animals. In all rats, I was able to observe that: (a) stable cells exhibited relatively consistent spatial representations across conditions in both CA1 and CA3, (b) global remapping in CA1 abruptly differentiated the pre-fog and fog blocks, and (c) CA1 place cells that exhibited global remapping maintained the changed firing patterns even when re-experiencing the original fog-free environment (i.e., fog-0%) in the fog block.

I found a significant increase in the firing rates of place cells that underwent global remapping in CA1 as the rat experienced the various fog conditions compared to the pre-fog baseline ($\chi^2_{(3)}$ = 99.44, p < 0.0001, Kruskal-Wallis test; pre-fog vs. fog-0%: Z = -8.12, p < 0.0001; pre-fog vs. fog-15%: Z = -8.29, p < 0.0001; pre-fog vs. fog-30%: Z = -7.85, p < 0.0001; fog-15% vs. fog-30%: Z = 1.28, p = 0.20, Wilcoxon rank-sum test) (**Figure 35A**). However, within the fog block, firing rates of place cells in CA1 that remapped globally were maintained at similar levels across different fog conditions ($\chi^2_{(2)}$ = 1.72, p = 0.4231, Kruskal-Wallis test) (**Figure 35A**). In contrast, the firing rates of stable place cells in CA1 did not change significantly compared with the pre-fog condition, not only for fog-0% (Z = -0.77, p = 0.4431, Wilcoxon rank-sum test) but also for fog-15% (Z = 0.20, p = 0.8416) and fog-30% (Z = 1.16, p = 0.2470) (**Figure 35B**). Unlike the case for global remapping cells, the firing rates of stable cells in CA1 significantly decreased as the fog became denser ($\chi^2_{(2)}$ = 13.43, p = 0.0012, Kruskal-Wallis test; 0% vs. 15%: Z = 1.91, p = 0.0556; 0% vs. 30%: Z = 3.35, p = 0.0008; 15% vs. 30%: Z = 2.34, p = 0.0191, Wilcoxon rank-sum test). In CA3, the firing rates of stable place cells decreased significantly across fog conditions ($\chi^2_{(3)}$ = 36.71, p < 0.0001, Kruskal-Wallis test; pre-fog vs. fog-0%: Z = 1.04, p = 0.2977; pre-fog vs. fog-15%: Z = 2.02, p = 0.0438; pre-fog vs. fog-30%: Z = 3.09, p = 0.0020; fog-15% vs. fog-30%: Z = 4.08, p < 0.0001; Wilcoxon rank-sum test) (**Figure 35C**).

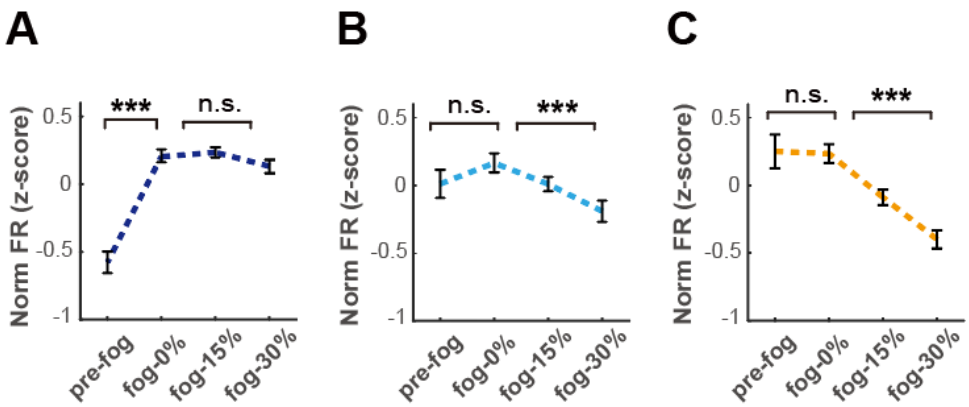

Figure 35. Normalized firing rates of place cells for each fog condition. (A-B): The normalized firing rates from (A) *CA1 global remapping* and (B) *CA1 stable* for each fog condition. The z-score was acquired from the firing rates across the fog % conditions within each cell. A subpopulation that underwent global remapping showed a significant increase in the firing rates from the fog % conditions (*** $p < 0.0001$). However, after the global remapping, they did not differ firing rates across the fog condition ($p = 0.7001$; Kruskal-Wallis test). In contrast, a significant rate reduction in *CA1 stable* was observed (*** $p < 0.0001$). (C): The normalized firing rates from *CA3 stable* for each fog condition. A significant firing rate reduction was observed in *CA3 stable* at the higher level of the fog % condition (*** $p < 0.0001$).

Overall, approximately half of place cells in CA1 remapped globally between pre-fog and fog conditions, and the other half (i.e., stable cells) maintained their fields without global remapping (**Figure 36)**. The global remapping place cells in CA1 did not show significant rate remapping according to the fog level once the fog block started, whereas the stable cells exhibited density-dependent rate remapping within the fog block. Such heterogeneous remapping patterns in CA1 were also found in CA3, but the majority of place cells (72.3%) in CA3 were stable (**Figure 36**).

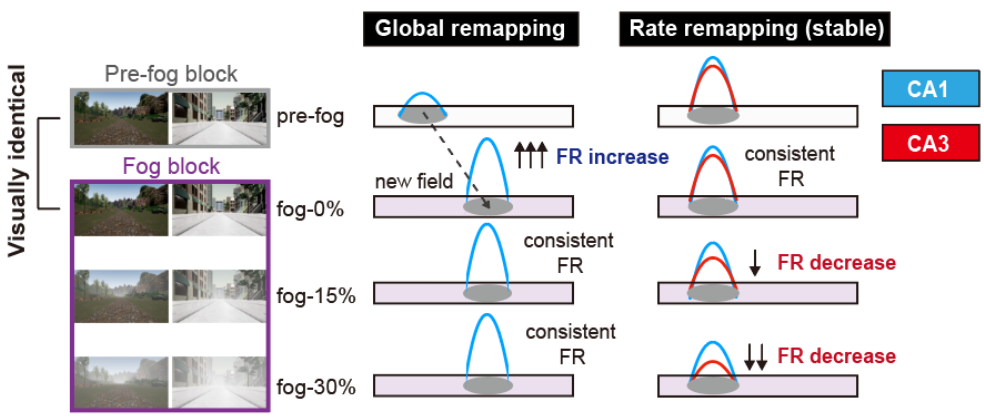

Figure 36. Schematic illustration of the global remapping and rate remapping (stable) place cells in CA1 and CA3 in fog-manipulation sessions. The place cells in CA1 were split into two subpopulations where they distinctively exhibited either global remapping or rate remapping at the subtle visual changes in the environment. The rate remapping cells in CA1 displayed similar firing patterns to the CA3 (**Figure 36B**; **Figure 36C**; rate remapping cells in both CA1 and CA3 showed a gradual decrease in firing rate according to the fog level). In contrast, global remapping cells showed

distinctively different firing patterns compared to rate remapping cells (**Figure 35A**; the firing rate of global remapping cells abruptly increased in fog conditions and maintained a similar level across the fog conditions). While these divisions of the remapping types have counted towards 'partial remapping' or 'heterogeneous remapping' in CA1 from the previous studies, I have separated those two remapping types within the same manipulation and systematically quantified their firing patterns upon the sensory change as well as contextual change.

Discussion

In the current study, I examined whether adding subtle visual noise to familiar and more enriched VR environments induced differential network behaviors in CA1 and CA3. In CA1, two heterogeneous subpopulations of place cells were identified: one that undergoes global remapping to distinguish the original environment from the foggy environment (i.e., fog block) and one that represents the local sensory changes (e.g., different densities of fog) within the fog block. Place cells in CA3 belonged to the latter class, suggesting that the stable cells in CA1 may be influenced by the CA3 network and perform mostly pattern completion when subtle sensory change is detected in the familiar environment. If one considers the global remapping subpopulation in CA1 to represent cells conducting pattern separation to encode contextual change, the heterogeneous subpopulations in CA1 may reflect the coexistence of pattern-completing and pattern-separating classes of place cells that mainly represent the original environment and the modified context, respectively. While prior studies have reported heterogeneous firing patterns of CA1 in response to various environmental modifications (Anderson and Jeffery, 2003; O'Keefe and Conway, 1978; Shapiro et al., 1997; Tanila et al., 1997), these results report the systematic observation of distinct functional subclasses of place cells in CA1, but not in CA3, in response to noisy inputs from the environment.

Global remapping and rate remapping of place cells have been associated with global geometric and sensory cue changes in the environment, respectively (Anderson and Jeffery, 2003; Leutgeb et al., 2005b). However, in this study, I was able to robustly induce global remapping by making only subtle changes in the visually enriched VR environment by introducing virtual fog, since the two VR environments (City and Forest) were based on identical geometric structures (e.g., the same linear track). These findings suggest that global remapping may occur whenever the hippocampus needs to construct a different cognitive map of the environment, such as one for the foggy environment. Previous studies showed that changes in environmental geometry may drive the hippocampus to form a new cognitive map (Colgin et al., 2010; Leutgeb et al., 2005b; Lever et al., 2002), but present findings suggest that this may not be the only condition that induces global remapping in the hippocampus.

Global remapping also occurred in the fog-0% condition. The fog-0% condition was physically identical to the original environment (pre-fog condition), suggesting that the introduction of the fog block may induce some global and top-down contextual change signals in the hippocampus. In support of this possibility, I found that introducing the fog manipulation elevated the rat's arousal level (**Figure 27**). It has been suggested that the release of acetylcholine within the brain may underlie the increase in arousal and attention (Everitt and Robbins, 1997; Hasselmo and Sarter, 2011). The cholinergic inputs innervate to the hippocampus from the medial septum

(Amaral and Kurz, 1985; Milner et al., 1983), and the increased acetylcholine may facilitate the induction of synaptic plasticity to enhance flexibility for encoding new information (Shinoe et al., 2005). These previous reports are supported by the observation that the global remapping cells gradually increased their firing rates as the rat experienced the fog trials (**Figure 29**). In addition, it has been demonstrated that acetylcholine prioritizes inputs from the entorhinal cortex to CA1 by regulating feedforward inhibitory circuits (Palacios-Filardo et al., 2021), which may underlie the abrupt global remapping in CA1 in the study. Taken together, these findings imply that the hippocampus may build multiple cognitive maps for the same environment, and this occurs more likely in CA1 than in CA3.

It is possible that the stable cells in CA1 were mostly driven by the same type of place cells (i.e., stable cells) in CA3, in which the majority of place cells also showed fog density-based rate remapping. Although cells showing rate remapping are present in CA1, global remapping may represent the default coding strategy of CA1 when the environment is modified, and this process may occur independently from that in CA3 (Dong et al., 2021). This reasoning is based on my observation that the proportion of place cells in CA1 is sensitive to the introduction of visual landmarks, with silent cells starting to fire on the track as visual landmarks were added one by one—a form of global remapping. If cells that showed rate remapping in CA1 were mostly driven by inputs from CA3, the

prediction is that CA1 might show only global remapping, but not rate remapping, if CA3 is blocked. Such functional relationships between the CA1 and CA3 subregions may explain recent experimental findings (Keinath et al., 2020; Zutshi et al., 2022).

General Discussion

The question, "How is episodic memory formed and sustained in the hippocampus?" is a general question among the learning and memory community. Starting from the broadest question, I aimed to address the answer by breaking the question down into specific ones: how do the hippocampal subregions CA1 and CA3 react to modifications in the environment that was previously known to be stable? Specifically, when there is a change in the stable environment, not only the sensory stimulus changes but also the modification itself can be counted as an event.

For instance, it would be remembered as a salient event if we could experience heavy snow in the tropical rainforest. From that point on, we might start to think that the rainforest we once knew is no longer always 'greenish' all year long. As such, environmental changes have the property of having the form of episodic memory containing elements of 'where,' 'what,' and 'when' in updating instantaneous stimulus changes as well as the meaning of the environment. Similarly, I created the circumstances where the animal encounters a discrepancy between the newly introduced visual noise on the environment from its prior knowledge.

It has been reported from the previous studies that, unlike the activities in which CA3 forms a discrete representation of the modified environment, CA1, which receives direct input from CA3, has shown a complex response according to environmental changes. In particular, 'partial

remapping,' in which global remapping and rate remapping are observed simultaneously, has been frequently observed in CA1, and its interpretation and meaning remained ambiguous. In this thesis, the rate remapping cell in CA1 can be interpreted as a pattern completion-like cell similar to those found in CA3. In contrast, the global remapping cell in CA1 can be interpreted as a pattern separation-like cell. These suggest that complex CA1 activities from the previous literature are information processed by certain rules with two types of cells unique to CA3 and other input, possibly EC3 (**Figure 37**).

Previous studies reported the activity of place cells with stimulus changes in the environment as an axis. Here, I would like to expand this axis further to interpret the activity of place cells. Until now, when measuring the activity of a place cell, the 'place' had been inseparable and also salient, so it might have been responded as if it were specifically bound to the place. In the similar line, an axis other than 'place' can also be aligned on that axis if it is important to animals. For example, even if someone is measuring the hippocampus activity of an animal foraging in the same space, the difference in how the animal perceives the space over time can also be an axis. In my thesis, this axis is defined as a 'context.'

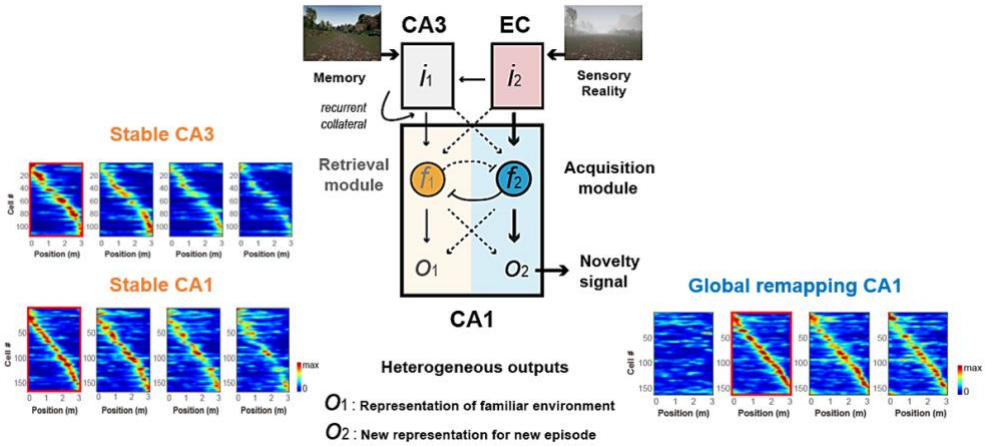

Figure 37. Working model of the hippocampal system in the mismatched condition. The place cells in CA1 were split into two subpopulations where they distinctively exhibited either global remapping or rate remapping at the subtle visual changes in the environment. In this working model, it is assumed in the model that there will be a module *f1* (i.e., recall module) and a module *f2* (i.e., acquisition module) in CA1, depending on the difference in synapse strength from CA3 or EC. If the expected sensory stimulus is processed in CA3 and the sensory stimulus comes from the EC match, the recall module will be dominantly activated. On the other hand, if the expected sensory stimulus and sensory stimulus do not match (i.e., fog block), the acquisition module will be activated to send novelty signals to the subcortical areas such as the ventral tegmental area (VTA), therefore, leading to the increased synaptic plasticity to encode new information.

Interpreting the place cell's activities as an axis other than space is not new, and the time cell can be interpreted as in the similar context (Eichenbaum, 2014). In addition, it has been reported that the place cells are selectively tuned to the specific sound frequency as form of a "Sound modulated cell" (Aronov et al., 2017), which is observed in animals that need to be lever pressed according to sound frequency, or a "VEVS cell" that responds to light bar movements (Purandare et al., 2022). In this thesis, I suggest that the global remapping and rate remapping types of place cell observed in CA1 have their own functions of either i) representing new episodes (i.e., context) in the environment or ii) representing sensory changes of the environment. In the broader context, for memories to be stable and flexible at the same time, there must be stable and flexible representations of neural networks in the brain. Here, I suggest the possibility that two distinct subpopulations in hippocampal CA1 manifest both stages with either flexible or stable representation without interfering with one another during the environmental change.

Meanwhile, the phenomenon that rate remapping responds to changes in the environment with a selective directionality (i.e., decrease) is an interesting phenomenon in this study. As the amount of noise level was increased in the environment, the rate reduction became more pronounced in both CA3 and CA1 rate remapping cells. In CA3, as a feature of an auto-associative network, if partial or noisy inputs that are similar to the existing representation enter, the memory is retrieved (i.e., pattern completion).

However, pattern completion and separation have been discussed in network patterns (e.g., on/off) of ensemble units, and this phenomenon can't be explained in this frame. As far as I know, there is no sufficient model for rate remapping, and its mechanism needs to be further investigated in the near future.

Functional-wise, we can imagine the possibility that uncertainty from the changing environment eventually tones down the network, or that could be a simple reduction from the loss of information within the noisy environment. While these possibilities can't be directly tested in my study design where the experiment was conducted by adding visual noise to the standard environment, but one can think of a new experimental design to test the above possibilities. For example, the naive animal never goes through the standard environment. Instead, they are trained with the Fog-30% condition for more than four days. After experiencing the Fog-30% condition environment as a baseline trial in the fog session, Fog-15%; Fog-0% are given in a pseudorandom manner. Here, if rate remapping shows a reduction in the firing rates, it suggests the possibility that uncertainty for the changing environment has been the major factor. On the other hand, if rate remapping shows an increase in the firing rates, it is possible to consider the possibility that the network was toned down due to the information content loss within the environment.

Overall, the introduction of visual noise caused global remapping and rate remapping of approximately 28% and 72%, respectively, of active

place cells in CA3. Meanwhile, given that CA3 also underwent some degree of global remapping and that both types of remapping theoretically require novelty detection, it is possible that mismatch detection occurs throughout the hippocampal subregions and is not necessarily specific to CA1 (Hasselmo and Schnell, 1994; McClelland et al., 1995) or CA3 (Vinogradova et al, 2001). Nonetheless, the different proportions of global remapping and rate remapping between CA1 and CA3 may suggest functional differences between the two subregions.

In particular, global remapping has been associated with more radical changes, thus higher discrepancy, of the environment (e.g., change in room geometry) compared with rate remapping (e.g., change in wall color). Although additional studies are required to determine whether the 50% of CA1 place cells that showed rate remapping in the noisy environment were entirely or partially driven by the 72% of rate remapping place cells in CA3, this particular ratio between global remapping and rate remapping cell populations may function as an index to indicate the network state that codes environmental changes. That is, downstream cortical structures of CA1 may consider the ratio between the proportions of CA1 cells showing global remapping and rate remapping to judge the situation as being a new environment or a novel episode in the same environment. In addition, DG-CA3 networks perform pattern completion and pattern separation on the basis of the quality and quantity of environment novelty (Lee and Lee,

2020), and their inputs to CA1 may also be crucial in determining such global-to-rate remapping ratios in CA1.

The global-to-rate remapping ratios in CA1 under different conditions may have contributed to the less coherent firing patterns of CA1 place cells compared to those from CA3, which have been consistently reported for the last few decades (Dong et al., 2021; Lee et al., 2004; Leutgeb et al., 2005b). This variability may be speculated to be produced by individual differences (Wills et al., 2005), the amount of prior experience (Colgin et al., 2010; Leutgeb et al., 2005b; Plitt and Giocomo, 2021; Wills et al., 2005), or the subjective belief of an environment (i.e., hidden state inference) (Sanders et al., 2020). However, unfortunately, in my experiment, the ratio of global remapping cells over four days was found to be consistent. Nevertheless, suppose the fog sessions were repeated over ten days for animals to perceive it as a daily routine. In that case, I predict that the proportion of global remapping cells will be decreased. This possibility should be tested in the near future.

Up to date, the less coherent firing patterns of CA1 place cells in response to environmental manipulations have been reported almost from the beginning of place cell research. For example, O'Keefe and Conway (1978) used an elevated T-maze inside a set of black curtains, where the rat had been trained for place discrimination. T-maze arms were specified by four cues (light, card, fan, and buzzer), and other cues were controlled by rotating the maze. Here, the authors reported for the first time that some

single units are excited by one or two cues while others are influenced in a more complex way. Later, these cells were termed either a 'concordant cell' or a 'discordant cell' by other research groups (Shapiro et al., 1997; Tanila et al., 1997). Moreover, when Muller and Kubie (1987) scaled the standard cylinder to increase the diameter and height of the environment by a factor of two, 36% of the cells observed in both cylinders also scaled their firing field, and the place field stayed at the same relative position. However, 52% of the cells displayed remarkably different firing patterns in the larger cylinder, presumably a global remapping.

In this context, Anderson and Jeffery (2003) also showed that the remapping patterns of place cells in CA1 should be interpreted as the combinatorial results of spatial and nonspatial environmental cues (so-called “stimulus modalities” in the study) with the most complex environmental manipulation eliciting the most remapping in CA1. The reports included the “split” of the population of CA1 place cells into global remapping and rate remapping subclasses in the same rats under the same conditions.

Similarly, whether the two distinct subpopulations in the CA1 observed in my study come from a ‘hard-wired’ network or to be a soft-wired network with flexible transition remains to be determined. Nevertheless, the division of the subpopulation within CA1 can be speculated to be produced from the deep and superficial layers (Sharif et al., 2021), the involvement of NMDA receptors in forming place fields (Sheffield et al., 2017), different plasticity mechanisms (Bittner et al., 2015;

Priestley et al., 2022), spike timing based on distinct inhibitory dynamics, such as those for parvalbumin vs. somatostatin (Fernandez-Ruiz et al., 2017; Royer et al., 2012). The abovementioned speculations altogether favor the possibility of a ‘hard-wired’ subpopulation in the CA1, and recent work demonstrating the segregation of the deep vs. superficial layer by the birthdate of the cell (Huszar et al., 2022) once more emphasizes the possibility. Furthermore, these cells with the same birthdate had a higher probability of having similar spatial fields compared to the cells with a different birthdate which leads to the phrase ‘neurons born together wire and fire together.’

Lastly, as I used a visually-enriched environment to monitor the activity of the place cells, I would like to emphasize the importance of the visual patterns (i.e., scene) in navigating rodents as well as the place cell activity. The rodent’s visual systems have evolved to adapt to the nocturnal environment since the rodent's retina consists primarily of rods to facilitate processing dim visual stimuli in dark conditions (Jacobs et al., 2001; LaVail, 1976). Furthermore, rodents lack the fovea in their eyes, perhaps focusing more on processing visual patterns as a whole instead of visually analyzing a particular area of the environment in great detail (Heffner and Heffner, 1992; Lashley, 1932). Thus, the rodent's visual acuity should be blurrier than that of ours and nonhuman primates. Visual acuity is measured in cycles per degree (*cpd*), which is the number of distinct lines that can be perceived within a degree of the subject's visual field. While the acuity of primates is

reported to be up to 60 *cpd* (Cronin, 2014; Spence, 1934), pigmented rats have a visual acuity of 0.95~1.6 *cpd* (Birch and Jacobs, 1979; Heffner and Heffner, 1992; Prusky et al., 2002; Seymoure and Juraska, 1997).

The rodent visual systems and their nocturnal behavioral conditions may mislead one to think that visual scenes are unimportant in their behavior. However, decades of prior studies have repeatedly shown that rodents use visual patterns in the background for spatial navigation and contextual information processing (Bussey et al., 2008; Carr, 1917; Forwood et al., 2007; Gaffan and Eacott, 1995; Higginson, 1926; Honzik, 1936; Lashley, 1930; Morris, 1981; Olton and Samuelson, 1976; Prusky et al., 2004; Tolman, 1939; Tolman and Minium, 1942; Vincent, 1915; Walthall Jr, 1948) as in humans and nonhuman primates. For example, Carr (1917) reported that rats trained in a maze lost their way if the maze was rotated, but if the visual cues were rotated along the maze, their performance was found to be intact (Higginson, 1926). Visual cues in mazes facilitate spatial learning in the environment (Walthall Jr, 1948), whereas removing visual cues results in a performance drop (Honzik, 1936).

Furthermore, Tolman and his colleagues trained rats to visually discriminate subsets of visual patterns (Lashley, 1930). When trained to choose one of the visual patterns, the rat's behavior was affected by the contrast difference in the visual patterns between the pair of visual patterns. That is, it took fewer days for rats to discriminate the easy stimuli (i.e., white versus black visual stimuli) than to learn the harder ones (i.e., white

versus grey or white versus light gray). Interestingly, their tendency to develop vicarious trial and error remained minimal for the easiest visual stimuli (Tolman, 1939; Tolman and Minium, 1942).

Further behavioral evidence showing the dependency of visual patterns in rodent spatial navigation was demonstrated in various mazes such as the radial arm maze (Olton and Samuelson, 1976), Barnes maze (Barnes, 1979), Cheeseboard maze (Gilbert and Kesner, 2002), Morris water maze (Morris, 1981), and T-maze (Packard and McGaugh, 1996; Tolman et al., 1946; 1947). Typically, when constructing the maze environment, it is well known that providing distal or allocentric cues should be placed on the walls of the room where the maze is placed to facilitate the spatial navigation of animals. Various forms of visual cues have been used, including simple gray curtains (Barnes, 1979), cue cards containing a pattern of vertical black and white stripes (Robinson et al., 2001), colored shapes (e.g., triangle or circle) (Sunyer et al., 2007), or complex visual patterns (e.g., posters, colorful geometric shapes; toys, etc.,) (Byun and Lee, 2010; Jo and Lee, 2010; Kim et al., 2011; Kim and Lee, 2011; Lee et al., 2005; Lee and Kim, 2010; Lee and Solivan, 2008; Suzuki et al., 1980). In a typical experimental setting, there are multiple (more than three) distal cues hung on the walls of the testing room (Jo and Lee, 2010; Kim et al., 2011; Kim and Lee, 2011; Lee et al., 2005; Lee and Kesner, 2004; Lee and Kim, 2010; Lee and Solivan, 2008; Lee et al., 2004; Pompl et al., 1999; Sunyer et al., 2007; Suzuki et al., 1980). When a laboratory room is used with

cluttered objects and furniture in the background, those naturally serve as visual cues (Hamilton et al., 2008; Hamilton et al., 2009; Sunyer et al., 2007).

The distal visual cues provided in the abovementioned maze environments are effective in spatial navigation because rodents use the visual scenes or patterns composed of those cues to orient themselves spatially and to find their positions. Gaffan and Eacott (1995) tested if rats use “visual patterns" more directly by training rats in a computer-controlled Y-maze. In their task, rats were required to discriminate between subsets of visual stimuli associated with rewards. Here, not only did rats successfully learn the associations between the visual stimuli with reward, but their training efficiency (i.e., the number of trials to successfully associate the rewarded stimuli) improved in the presence of complex visual patterns (i.e., scenes such as varying numbers of geometric shapes distributed throughout the monitor screen) than in the presence of objects (homogeneous single figures, primarily displayed on the central part of the screen) (Gaffan and Eacott, 1995). Similar studies using visual patterns projected on computer monitors as *discriminanda* in rodents verified that rats are effective in using allocentrically presented visual patterns for decision making (Bussey et al., 2008; Forwood et al., 2007; Prusky et al., 2002; Prusky et al., 2000).

What would be the role of the hippocampal system in producing such adaptive behaviors using visual scenes? There have been numerous studies demonstrating the necessity of the hippocampus and its associated

areas in forming and retrieving scene-based memories (Gaffan et al., 2001; Gaffan and Eacott, 1997; Kim et al., 2012; Park et al., 2017; Park et al., 2022; Prusky et al., 2004; Simpson et al., 1998; Yoo and Lee, 2017). For example, in a spatial navigation task using a radial arm maze in which animals were required to visit the arms baited with rewards using extra-maze cues, the rats with lesions in the hippocampi were impaired in the initial acquisition of the task (Jarrard, 1978; Jarrard, 1986; Morris et al., 1982). Also, it has been demonstrated that hippocampal lesions abolish fear responses associated with a polymodal context but not with a simple elemental stimulus such as a pure tone (Kim and Fanselow, 1992). Despite the lack of demand for spatial navigation, the necessity of the hippocampus in contextual fear conditioning (Kim and Fanselow, 1992; Phillips and LeDoux, 1994) strongly suggests that the hippocampus is directly involved in associating visual scenes with specific adaptive behaviors. Visual patterns appear to incorporate the hippocampus in humans and are essential for eliciting place cells in rodents. However, the activity of the place cell should not be understood as a simple perceptual response but rather as a complex mnemonic process in which the events based on the sensory environments are stitched together. Most importantly, identifying what has been changed in the visual patterns should be essential to guide adaptive behavior in a dynamic environment.

Bibliography

Acharya, L., Aghajan, Z.M., Vuong, C., Moore, J.J., and Mehta, M.R. (2016). Causal Influence of Visual Cues on Hippocampal Directional Selectivity. Cell 164, 197-207.

Allen, K., Rawlins, J.N., Bannerman, D.M., and Csicsvari, J. (2012). Hippocampal place cells can encode multiple trial-dependent features through rate remapping. J Neurosci 32, 14752-14766.

Allen, T.A., and Fortin, N.J. (2013). The evolution of episodic memory. Proc Natl Acad Sci U S A 110 Suppl 2, 10379-10386.

Amaral, D.G., Ishizuka, N., and Claiborne, B. (1990). Neurons, numbers and the hippocampal network. Prog Brain Res 83, 1-11.

Amaral, D.G., and Kurz, J. (1985). An analysis of the origins of the cholinergic and noncholinergic septal projections to the hippocampal formation of the rat. J Comp Neurol 240, 37-59.

Amaral, D.G., and Witter, M.P. (1989). The three-dimensional organization of the hippocampal formation: a review of anatomical data. Neuroscience 31, 571-591.

Anderson P, Bliss TV, Lomo T, Olsen LI, Skrede KK (1969). Lamellar organization of hippocampal excitatory pathways. Acta Physiol Scand 76:4A-5A.

Anderson, M.I., and Jeffery, K.J. (2003). Heterogeneous modulation of place cell firing by changes in context. J Neurosci 23, 8827-8835.

Aronov, D., Nevers, R., and Tank, D.W. (2017). Mapping of a non-spatial dimension by the hippocampal-entorhinal circuit. Nature 543, 719-722.

Aronov, D., and Tank, D.W. (2014). Engagement of neural circuits underlying 2D spatial navigation in a rodent virtual reality system. Neuron 84, 442-456.

Bains, J.S., Longacher, J.M., and Staley, K.J. (1999). Reciprocal interactions between CA3 network activity and strength of recurrent collateral synapses. Nat Neurosci 2, 720-726.

Barnes, C.A. (1979). Memory deficits associated with senescence: a neurophysiological and behavioral study in the rat. J Comp Physiol Psychol 93, 74-104.

Birch, D., and Jacobs, G.H. (1979). Spatial Contrast Sensitivity in Albino and Pigmented Rats. Vision Research 19, 933-937.

Bittner, K.C., Grienberger, C., Vaidya, S.P., Milstein, A.D., Macklin, J.J., Suh, J., Tonegawa, S., and Magee, J.C. (2015). Conjunctive input processing drives feature selectivity in hippocampal CA1 neurons. Nat Neurosci 18, 1133-1142.

Boss, B.D., Peterson, G.M., and Cowan, W.M. (1985). On the number of neurons in the dentate gyrus of the rat. Brain Res 338, 144-150.

Bostock, E., Muller, R.U., and Kubie, J.L. (1991). Experience-dependent modifications of hippocampal place cell firing. Hippocampus 1, 193-205.

Bourboulou, R., Marti, G., Michon, F.X., El Feghaly, E., Nouguier, M., Robbe, D., Koenig, J., and Epsztein, J. (2019). Dynamic control of hippocampal spatial coding resolution by local visual cues. Elife 8.

Bussey, T.J., Padain, T.L., Skillings, E.A., Winters, B.D., Morton, A.J., and Saksida, L.M. (2008). The touchscreen cognitive testing method for rodents: How to get the best out of your rat. Learn Memory 15, 516-523.

Byun, J., and Lee, I. (2010). Disambiguation of similar object-place paired associations and the roles of the brain structures in the medial temporal lobe. Exp Neurobiol 19, 15-22.

Carr, H. (1917). Maze studies with the white rat. Journal of Animal Behavior 7, 259-275.

Chen, G., King, J.A., Burgess, N., and O'Keefe, J. (2013). How vision and movement combine in the hippocampal place code. Proc Natl Acad Sci U S A 110, 378-383.

Chen, G., Lu, Y., King, J.A., Cacucci, F., and Burgess, N. (2019). Differential influences of environment and self-motion on place and grid cell firing. Nat Commun 10, 630.

Churchland, P.S., and Sejnowski, T.J. (1992). The computational brain (MIT Press).

Claiborne, B.J., Amaral, D.G., and Cowan, W.M. (1990). Quantitative, three-dimensional analysis of granule cell dendrites in the rat dentate gyrus. J Comp Neurol 302, 206-219.

Cohen, J.D., Bolstad, M., and Lee, A.K. (2017). Experience-dependent shaping of hippocampal CA1 intracellular activity in novel and familiar environments. Elife 6.

Colgin, L.L., Leutgeb, S., Jezek, K., Leutgeb, J.K., Moser, E.I., McNaughton, B.L., and Moser, M.B. (2010). Attractor-map versus autoassociation based attractor dynamics in the hippocampal network. J Neurophysiol 104, 35-50.

Colgin, L.L., Moser, E.I., and Moser, M.B. (2008). Understanding memory through hippocampal remapping. Trends Neurosci 31, 469-477.

Cronin, T.W. (2014). Visual ecology (Princeton University Press).

Cushman, J.D., Aharoni, D.B., Willers, B., Ravassard, P., Kees, A., Vuong, C., Popeney, B., Arisaka, K., and Mehta, M.R. (2013). Multisensory control of multimodal behavior: do the legs know what the tongue is doing? PLoS One 8, e80465.

de No RL (1934). Studies on the struture of the cerebral cortex XI Continuation of the sutdy of the ammonic system. J Psychol Neurol 46:113-177.

Debanne, D., Gahwiler, B.H., and Thompson, S.M. (1998). Long-term synaptic plasticity between pairs of individual CA3 pyramidal cells in rat hippocampal slice cultures. J Physiol 507 (Pt 1), 237-247.

Delcasso, S., Huh, N., Byeon, J.S., Lee, J., Jung, M.W., and Lee, I. (2014). Functional relationships between the hippocampus and dorsomedial striatum in learning a visual scene-based memory task in rats. J

Neurosci 34, 15534-15547.

Deshmukh, S.S. (2021). Distal CA1 Maintains a More Coherent Spatial Representation than Proximal CA1 When Local and Global Cues Conflict. J Neurosci 41, 9767-9781.

Dong, C., Madar, A.D., and Sheffield, M.E.J. (2021). Distinct place cell dynamics in CA1 and CA3 encode experience in new environments. Nat Commun 12, 2977.

Eichenbaum, H. (2000). A cortical-hippocampal system for declarative memory. Nat Rev Neurosci 1, 41-50.

Eichenbaum, H. (2014). Time cells in the hippocampus: a new dimension for mapping memories. Nat Rev Neurosci 15, 732-744.

Ekstrom, A.D., Kahana, M.J., Caplan, J.B., Fields, T.A., Isham, E.A., Newman, E.L., and Fried, I. (2003). Cellular networks underlying human spatial navigation. Nature 425, 184-188.

Epsztein, J., Brecht, M., and Lee, A.K. (2011). Intracellular determinants of hippocampal CA1 place and silent cell activity in a novel environment. Neuron 70, 109-120.

Everitt, B.J., and Robbins, T.W. (1997). Central cholinergic systems and cognition. Annu Rev Psychol 48, 649-684.

Felleman, D.J., and Van Essen, D.C. (1991). Distributed hierarchical processing in the primate cerebral cortex. Cereb Cortex 1, 1-47.

Fenton, A.A., Csizmadia, G., and Muller, R.U. (2000). Conjoint control of hippocampal place cell firing by two visual stimuli. Ii. A vector-field

theory that predicts modifications of the representation of the environment. J Gen Physiol 116, 211-221.

Fenton, A.A., Kao, H.Y., Neymotin, S.A., Olypher, A., Vayntrub, Y., Lytton, W.W., and Ludvig, N. (2008). Unmasking the CA1 ensemble place code by exposures to small and large environments: more place cells and multiple, irregularly arranged, and expanded place fields in the larger space. J Neurosci 28, 11250-11262.

Ferbinteanu, J., and Shapiro, M.L. (2003). Prospective and retrospective memory coding in the hippocampus. Neuron 40, 1227-1239.

Fernandez-Ruiz, A., Oliva, A., Nagy, G.A., Maurer, A.P., Berenyi, A., and Buzsaki, G. (2017). Entorhinal-CA3 Dual-Input Control of Spike Timing in the Hippocampus by Theta-Gamma Coupling. Neuron 93, 1213-1226 e1215.

Flicker, C., and Geyer, M.A. (1982). Behavior during hippocampal microinfusions. I. Norepinephrine and diversive exploration. Brain Res 257, 79-103.

Forwood, S.E., Bartko, S.J., Saksida, L.M., and Bussey, T.J. (2007). Rats spontaneously discriminate purely visual, two-dimensional stimuli in tests of recognition memory and perceptual oddity. Behav Neurosci 121, 1032-1042.

Fyhn, M., Hafting, T., Treves, A., Moser, M.B., and Moser, E.I. (2007). Hippocampal remapping and grid realignment in entorhinal cortex. Nature 446, 190-194.

Gaffan, E.A., Bannerman, D.M., Warburton, E.C., and Aggleton, J.P. (2001). Rats' processing of visual scenes: effects of lesions to fornix, anterior thalamus, mamillary nuclei or the retrohippocampal region. Behav Brain Res 121, 103-117.

Gaffan, E.A., and Eacott, M.J. (1995). A computer-controlled maze environment for testing visual memory in the rat. J Neurosci Methods 60, 23-37.

Gaffan, E.A., and Eacott, M.J. (1997). Spatial memory impairment in rats with fornix transection is not accompanied by a simple encoding deficit for directions of objects in visual space. Behav Neurosci 111, 937-954.

Gilbert, P.E., and Kesner, R.P. (2002). Role of rodent hippocampus in paired-associate learning involving associations between a stimulus and a spatial location. Behav Neurosci 116, 63-71.

Gold, A.E., and Kesner, R.P. (2005). The Role of the CA3 Subregion of the Dorsal Hippocampus in Spatial Pattern Completion in the Rat. Hippocampus 15, 808-814.

Gonzales, R.B., DeLeon Galvan, C.J., Rangel, Y.M., and Claiborne, B.J. (2001). Distribution of thorny excrescences on CA3 pyramidal neurons in the rat hippocampus. J Comp Neurol 430, 357-368.

Gothard, K.M., Skaggs, W.E., and McNaughton, B.L. (1996). Dynamics of mismatch correction in the hippocampal ensemble code for space: Interaction between path integration and environmental cues. Journal

of Neuroscience 16, 8027-8040.

Gulli, R.A., Duong, L.R., Corrigan, B.W., Doucet, G., Williams, S., Fusi, S., and Martinez-Trujillo, J.C. (2020). Context-dependent representations of objects and space in the primate hippocampus during virtual navigation. Nat Neurosci 23, 103-112.

Hamilton, D.A., Akers, K.G., Johnson, T.E., Rice, J.P., Candelaria, F.T., Sutherland, R.J., Weisend, M.P., and Redhead, E.S. (2008). The relative influence of place and direction in the Morris water task. J Exp Psychol Anim Behav Process 34, 31-53.

Hamilton, D.A., Johnson, T.E., Redhead, E.S., and Verney, S.P. (2009). Control of rodent and human spatial navigation by room and apparatus cues. Behav Processes 81, 154-169.

Harvey, C.D., Collman, F., Dombeck, D.A., and Tank, D.W. (2009). Intracellular dynamics of hippocampal place cells during virtual navigation. Nature 461, 941-946.

Hasselmo, M.E., and Sarter, M. (2011). Modes and models of forebrain cholinergic neuromodulation of cognition. Neuropsychopharmacology 36, 52-73.

Hasselmo, M.E., and Schnell, E. (1994). Laminar selectivity of the cholinergic suppression of synaptic transmission in rat hippocampal region CA1: computational modeling and brain slice physiology. J Neurosci 14, 3898-3914.

Hasselmo, M.E., Wyble, B.P., and Wallenstein, G.V. (1996). Encoding and

retrieval of episodic memories: role of cholinergic and GABAergic modulation in the hippocampus. Hippocampus 6, 693-708.

Heffner, R.S., and Heffner, H.E. (1992). Visual factors in sound localization in mammals. J Comp Neurol 317, 219-232.

Henriksen, E.J., Colgin, L.L., Barnes, C.A., Witter, M.P., Moser, M.B., and Moser, E.I. (2010). Spatial representation along the proximodistal axis of CA1. Neuron 68, 127-137.

Hetherington, P.A., and Shapiro, M.L. (1997). Hippocampal place fields are altered by the removal of single visual cues in a distance-dependent manner. Behav Neurosci 111, 20-34.

Higginson, G.D. (1926). Visual perception in the white rat. Journal of Experimental Psychology 9, 337-347.

Hollup, S.A., Molden, S., Donnett, J.G., Moser, M.B., and Moser, E.I. (2001). Accumulation of hippocampal place fields at the goal location in an annular watermaze task. J Neurosci 21, 1635-1644.

Holscher, C., Schnee, A., Dahmen, H., Setia, L., and Mallot, H.A. (2005). Rats are able to navigate in virtual environments. J Exp Biol 208, 561-569.

Honey, R.C., Watt, A., and Good, M. (1998). Hippocampal lesions disrupt an associative mismatch process. J Neurosci 18, 2226-2230.

Honzik, C.H. (1936). The sensory basis of maze learning in rats. Comparative Psychology Monographs 13, 113-113.

Huszar, R., Zhang, Y., Blockus, H., and Buzsaki, G. (2022). Preconfigured

dynamics in the hippocampus are guided by embryonic birthdate and rate of neurogenesis. Nat Neurosci 25, 1201-1212.

Ishizuka, N., Weber, J., and Amaral, D.G. (1990). Organization of intrahippocampal projections originating from CA3 pyramidal cells in the rat. J Comp Neurol 295, 580-623.

Jacobs, G.H., Fenwick, J.A., and Williams, G.A. (2001). Cone-based vision of rats for ultraviolet and visible lights. J Exp Biol 204, 2439-2446.

Jarrard, L.E. (1978). Selective hippocampal lesions: differential effects on performance by rats of a spatial task with preoperative versus postoperative training. J Comp Physiol Psychol 92, 1119-1127.

Jarrard, L.E. (1986). Selective Hippocampal Lesions and Behavior. In The Hippocampus: Volume 4, R.L. Isaacson, and K.H. Pribram, eds. (Springer US), pp. 93-126.

Jo, Y.S., and Lee, I. (2010). Disconnection of the hippocampal-perirhinal cortical circuits severely disrupts object-place paired associative memory. J Neurosci 30, 9850-9858.

Jo, Y.S., Park, E.H., Kim, I.H., Park, S.K., Kim, H., Kim, H.T., and Choi, J.S. (2007). The medial prefrontal cortex is involved in spatial memory retrieval under partial-cue conditions. J Neurosci 27, 13567-13578.

Jung, M.W., Wiener, S.I., and McNaughton, B.L. (1994). Comparison of spatial firing characteristics of units in dorsal and ventral hippocampus of the rat. J Neurosci 14, 7347-7356.

Keinath, A.T., Nieto-Posadas, A., Robinson, J.C., and Brandon, M.P. (2020). DG-CA3 circuitry mediates hippocampal representations of latent information. Nat Commun 11, 3026.

Kentros, C., Hargreaves, E., Hawkins, R.D., Kandel, E.R., Shapiro, M., and Muller, R.V. (1998). Abolition of long-term stability of new hippocampal place cell maps by NMDA receptor blockade. Science 280, 2121-2126.

Kim, J., Delcasso, S., and Lee, I. (2011). Neural correlates of object-in-place learning in hippocampus and prefrontal cortex. J Neurosci 31, 16991-17006.

Kim, J., and Lee, I. (2011). Hippocampus is necessary for spatial discrimination using distal cue-configuration. Hippocampus 21, 609-621.

Kim, J.J., and Fanselow, M.S. (1992). Modality-specific retrograde amnesia of fear. Science 256, 675-677.

Kim, S., Lee, J., and Lee, I. (2012). The hippocampus is required for visually cued contextual response selection, but not for visual discrimination of contexts. Front Behav Neurosci 6, 66.

Knierim, J.J., Kudrimoti, H.S., and McNaughton, B.L. (1998). Interactions between idiothetic cues and external landmarks in the control of place cells and head direction cells. Journal of Neurophysiology 80, 425-446.

Knierim, J.J., and Rao, G. (2003). Distal landmarks and hippocampal place

cells: effects of relative translation versus rotation. Hippocampus 13, 604-617.

Lashley, K.S. (1930). The mechanism of vision: I. A method for rapid analysis of pattern-vision in the rat. The Pedagogical Seminary and Journal of Genetic Psychology 37, 453-460.

Lashley, K.S. (1932). The mechanism of vision V The structure and image-forming power of the rat's eye. J Comp Psychol 13, 173-200.

LaVail, M.M. (1976). Rod outer segment disc shedding in relation to cyclic lighting. Exp Eye Res 23, 277-280.

Lee, C.H., and Lee, I. (2020). Impairment of Pattern Separation of Ambiguous Scenes by Single Units in the CA3 in the Absence of the Dentate Gyrus. J Neurosci 40, 3576-3590.

Lee, C.H., Ryu, J., Lee, S.H., Kim, H., and Lee, I. (2016). Functional Cross-Hemispheric Shift Between Object-Place Paired Associate Memory and Spatial Memory in the Human Hippocampus. Hippocampus 26, 1061-1077.

Lee, H.W., Lee, S.M., and Lee, I. (2018). Neural Firing Patterns Are More Schematic and Less Sensitive to Changes in Background Visual Scenes in the Subiculum than in the Hippocampus. J Neurosci 38, 7392-7408.

Lee, I., Griffin, A.L., Zilli, E.A., Eichenbaum, H., and Hasselmo, M.E. (2006). Gradual translocation of spatial correlates of neuronal firing in the hippocampus toward prospective reward locations. Neuron 51,

639-650.

Lee, I., Hunsaker, M.R., and Kesner, R.P. (2005). The role of hippocampal subregions in detecting spatial novelty. Behav Neurosci 119, 145-153.

Lee, I., and Kesner, R.P. (2004). Encoding versus retrieval of spatial memory: Double dissociation between the dentate gyrus and the perforant path inputs into CA3 in the dorsal hippocampus. Hippocampus 14, 66-76.

Lee, I., and Kim, J. (2010). The shift from a response strategy to object-in-place strategy during learning is accompanied by a matching shift in neural firing correlates in the hippocampus. Learn Mem 17, 381-393.

Lee, I., and Solivan, F. (2008). The roles of the medial prefrontal cortex and hippocampus in a spatial paired-association task. Learn Mem 15, 357-367.

Lee, I., Yoganarasimha, D., Rao, G., and Knierim, J.J. (2004). Comparison of population coherence of place cells in hippocampal subfields CA1 and CA3. Nature 430, 456-459.

Leutgeb, J.K., Leutgeb, S., Moser, M.B., and Moser, E.I. (2007). Pattern separation in the dentate gyrus and CA3 of the hippocampus. Science 315, 961-966.

Leutgeb, J.K., Leutgeb, S., Treves, A., Meyer, R., Barnes, C.A., McNaughton, B.L., Moser, M.B., and Moser, E.I. (2005a). Progressive transformation of hippocampal neuronal representations

in "morphed" environments. Neuron 48, 345-358.

Leutgeb, S., Leutgeb, J.K., Barnes, C.A., Moser, E.I., McNaughton, B.L., and Moser, M.B. (2005b). Independent codes for spatial and episodic memory in hippocampal neuronal ensembles. Science 309, 619-623.

Lever, C., Wills, T., Cacucci, F., Burgess, N., and O'Keefe, J. (2002). Long-term plasticity in hippocampal place-cell representation of environmental geometry. Nature 416, 90-94.

Li, X.G., Somogyi, P., Ylinen, A., and Buzsaki, G. (1994). The hippocampal CA3 network: an in vivo intracellular labeling study. J Comp Neurol 339, 181-208.

Lisman, J.E., and Grace, A.A. (2005). The hippocampal-VTA loop: controlling the entry of information into long-term memory. Neuron 46, 703-713.

MacDonald, C.J., Lepage, K.Q., Eden, U.T., and Eichenbaum, H. (2011). Hippocampal "time cells" bridge the gap in memory for discontiguous events. Neuron 71, 737-749.

Markus, E.J., Barnes, C.A., McNaughton, B.L., Gladden, V.L., and Skaggs, W.E. (1994). Spatial information content and reliability of hippocampal CA1 neurons: effects of visual input. Hippocampus 4, 410-421.

Markus, E.J., Qin, Y.L., Leonard, B., Skaggs, W.E., Mcnaughton, B.L., and Barnes, C.A. (1995). Interactions between Location and Task Affect the Spatial and Directional Firing of Hippocampal-Neurons. Journal

of Neuroscience 15, 7079-7094.

Marr, D. (1971). Simple memory: a theory for archicortex. Philos Trans R Soc Lond B Biol Sci 262, 23-81.

McClelland, J.L., McNaughton, B.L., and O'Reilly, R.C. (1995). Why there are complementary learning systems in the hippocampus and neocortex: insights from the successes and failures of connectionist models of learning and memory. Psychol Rev 102, 419-457.

Milner, T.A., Loy, R., and Amaral, D.G. (1983). An anatomical study of the development of the septo-hippocampal projection in the rat. Brain Res 284, 343-371.

Mizuseki, K., Royer, S., Diba, K., and Buzsaki, G. (2012). Activity dynamics and behavioral correlates of CA3 and CA1 hippocampal pyramidal neurons. Hippocampus 22, 1659-1680.

Morris, R.G.M. (1981). SPATIAL LOCALIZATION DOES NOT REQUIRE THE PRESENCE OF LOCAL CUES. Learning and Motivation 12, 239-260.

Morris, R.G.M., Garrud, P., Rawlins, J.N.P., and Okeefe, J. (1982). Place Navigation Impaired in Rats with Hippocampal-Lesions. Nature 297, 681-683.

Muller, R.U., and Kubie, J.L. (1987). The effects of changes in the environment on the spatial firing of hippocampal complex-spike cells. J Neurosci 7, 1951-1968.

Muller, R.U., Kubie, J.L., and Ranck, J.B., Jr. (1987). Spatial firing patterns

of hippocampal complex-spike cells in a fixed environment. J Neurosci 7, 1935-1950.

Nakazawa, K., Quirk, M.C., Chitwood, R.A., Watanabe, M., Yeckel, M.F., Sun, L.D., Kato, A., Carr, C.A., Johnston, D., Wilson, M.A., and Tonegawa, S. (2002). Requirement for hippocampal CA3 NMDA receptors in associative memory recall. Science 297, 211-218.

Neunuebel, J.P., and Knierim, J.J. (2014). CA3 retrieves coherent representations from degraded input: direct evidence for CA3 pattern completion and dentate gyrus pattern separation. Neuron 81, 416-427.

Neunuebel, J.P., Yoganarasimha, D., Rao, G., and Knierim, J.J. (2013). Conflicts between Local and Global Spatial Frameworks Dissociate Neural Representations of the Lateral and Medial Entorhinal Cortex (May, pg 9246, 2013). Journal of Neuroscience 33, 13249-13249.

O'Keefe, J. (1976). Place units in the hippocampus of the freely moving rat. Exp Neurol 51, 78-109.

O'Keefe, J., and Conway, D.H. (1978). Hippocampal place units in the freely moving rat: why they fire where they fire. Exp Brain Res 31, 573-590.

O'Keefe, J., and Dostrovsky, J. (1971). The hippocampus as a spatial map. Preliminary evidence from unit activity in the freely-moving rat. Brain Res 34, 171-175.

O'Keefe, J., and Nadel, L. (1978). The hippocampus as a cognitive map

(Clarendon Press ;Oxford University Press).

O'Reilly, R.C., and McClelland, J.L. (1994). Hippocampal conjunctive encoding, storage, and recall: avoiding a trade-off. Hippocampus 4, 661-682.

Olton, D.S., and Samuelson, R.J. (1976). Remembrance of places passed: Spatial memory in rats. Journal of Experimental Psychology: Animal Behavior Processes 2, 97-116.

Packard, M.G., and McGaugh, J.L. (1996). Inactivation of hippocampus or caudate nucleus with lidocaine differentially affects expression of place and response learning. Neurobiol Learn Mem 65, 65-72.

Palacios-Filardo, J., Udakis, M., Brown, G.A., Tehan, B.G., Congreve, M.S., Nathan, P.J., Brown, A.J.H., and Mellor, J.R. (2021). Acetylcholine prioritises direct synaptic inputs from entorhinal cortex to CA1 by differential modulation of feedforward inhibitory circuits. Nat Commun 12, 5475.

Park, E.-H., Ahn, J.-R., and Lee, I. (2017). Interactions between stimulus and response types are more strongly represented in the entorhinal cortex than in its upstream regions in rats. eLife 6, e32657.

Park, S.-B., Lim, H.-Y., Lee, E.-Y., Yoo, S.-W., Jung, H.-S., Lee, E., Sun, W., and Lee, I. (2022). The fasciola cinereum subregion of the hippocampus is important for the acquisition of visual contextual memory. Progress in Neurobiology 210, 102217.

Park, S.B., and Lee, I. (2016). Increased Variability and Asymmetric

Expansion of the Hippocampal Spatial Representation in a Distal Cue-Dependent Memory Task. Hippocampus 26, 1033-1050.

Paxinos, G., and Watson, C. (2009). The Rat Brain in Stereotaxic Coordianates, 6th Edition (Elsevier).

Phillips, R.G., and LeDoux, J.E. (1994). Lesions of the dorsal hippocampal formation interfere with background but not foreground contextual fear conditioning. Learn Memory 1, 34-44.

Plitt, M.H., and Giocomo, L.M. (2021). Experience-dependent contextual codes in the hippocampus. Nat Neurosci 24, 705-714.

Pompl, P.N., Mullan, M.J., Bjugstad, K., and Arendash, G.W. (1999). Adaptation of the circular platform spatial memory task for mice: use in detecting cognitive impairment in the APP(SW) transgenic mouse model for Alzheimer's disease. J Neurosci Methods 87, 87-95.

Priestley, J.B., Bowler, J.C., Rolotti, S.V., Fusi, S., and Losonczy, A. (2022). Signatures of rapid plasticity in hippocampal CA1 representations during novel experiences. Neuron 110, 1978-1992 e1976.

Prusky, G.T., Douglas, R.M., Nelson, L., Shabanpoor, A., and Sutherland, R.J. (2004). Visual memory task for rats reveals an essential role for hippocampus and perirhinal cortex. Proc Natl Acad Sci U S A 101, 5064-5068.

Prusky, G.T., Harker, K.T., Douglas, R.M., and Whishaw, I.Q. (2002). Variation in visual acuity within pigmented, and between pigmented and albino rat strains. Behavioural Brain Research 136, 339-348.

Prusky, G.T., West, P.W., and Douglas, R.M. (2000). Behavioral assessment of visual acuity in mice and rats. Vision Res 40, 2201-2209.

Purandare, C.S., Dhingra, S., Rios, R., Vuong, C., To, T., Hachisuka, A., Choudhary, K., and Mehta, M.R. (2022). Moving bar of light evokes vectorial spatial selectivity in the immobile rat hippocampus. Nature 602, 461-467.

Radvansky, B.A., Oh, J.Y., Climer, J.R., and Dombeck, D.A. (2021). Behavior determines the hippocampal spatial mapping of a multisensory environment. Cell Rep 36, 109444.

Ramon y Cajal S (1983). Estructura del asta de Ammon y fascia dentata. Madrid: Tip. de Fortanet.

Ravassard, P., Kees, A., Willers, B., Ho, D., Aharoni, D.A., Cushman, J., Aghajan, Z.M., and Mehta, M.R. (2013). Multisensory control of hippocampal spatiotemporal selectivity. Science 340, 1342-1346.

Rich, P.D., Liaw, H.P., and Lee, A.K. (2014). Place cells. Large environments reveal the statistical structure governing hippocampal representations. Science 345, 814-817.

Rikhye, R.V., and Sur, M. (2015). Spatial Correlations in Natural Scenes Modulate Response Reliability in Mouse Visual Cortex. J Neurosci 35, 14661-14680.

Robinson, L., Bridge, H., and Riedel, G. (2001). Visual discrimination learning in the water maze: a novel test for visual acuity. Behav Brain Res 119, 77-84.

Rolls, E.T. (2010). A computational theory of episodic memory formation in the hippocampus. Behav Brain Res 215, 180-196.

Rolls, E.T. (2013). The mechanisms for pattern completion and pattern separation in the hippocampus. Front Syst Neurosci 7, 74.

Rolls, E.T., and Kesner, R.P. (2006). A computational theory of hippocampal function, and empirical tests of the theory. Prog Neurobiol 79, 1-48.

Rotenberg, A., and Muller, R.U. (1997). Variable place-cell coupling to a continuously viewed stimulus: evidence that the hippocampus acts as a perceptual system. Philos T R Soc B 352, 1505-1513.

Royer, S., Zemelman, B.V., Losonczy, A., Kim, J., Chance, F., Magee, J.C., and Buzsaki, G. (2012). Control of timing, rate and bursts of hippocampal place cells by dendritic and somatic inhibition. Nat Neurosci 15, 769-775.

Saleem, A.B., Diamanti, E.M., Fournier, J., Harris, K.D., and Carandini, M. (2018). Coherent encoding of subjective spatial position in visual cortex and hippocampus. Nature 562, 124-127.

Sanders, H., Wilson, M.A., and Gershman, S.J. (2020). Hippocampal remapping as hidden state inference. Elife 9.

Sato, M., Kawano, M., Mizuta, K., Islam, T., Lee, M.G., and Hayashi, Y. (2017). Hippocampus-Dependent Goal Localization by Head-Fixed Mice in Virtual Reality. eNeuro 4.

Save, E., Nerad, L., and Poucet, B. (2000). Contribution of multiple sensory information to place field stability in hippocampal place cells.

Hippocampus 10, 64-76.

Seymoure, P., and Juraska, J.M. (1997). Vernier and grating acuity in adult hooded rats: the influence of sex. Behav Neurosci 111, 792-800.

Shapiro, M.L., Tanila, H., and Eichenbaum, H. (1997). Cues that hippocampal place cells encode: Dynamic and hierarchical representation of local and distal stimuli. Hippocampus 7, 624-642.

Sharif, F., Tayebi, B., Buzsaki, G., Royer, S., and Fernandez-Ruiz, A. (2021). Subcircuits of Deep and Superficial CA1 Place Cells Support Efficient Spatial Coding across Heterogeneous Environments. Neuron 109, 363-376 e366.

Sheffield, M.E.J., Adoff, M.D., and Dombeck, D.A. (2017). Increased Prevalence of Calcium Transients across the Dendritic Arbor during Place Field Formation. Neuron 96, 490-504 e495.

Shinoe, T., Matsui, M., Taketo, M.M., and Manabe, T. (2005). Modulation of synaptic plasticity by physiological activation of M1 muscarinic acetylcholine receptors in the mouse hippocampus. J Neurosci 25, 11194-11200.

Simpson, E.L., Gaffan, E.A., and Eacott, M.J. (1998). Rats' object-in-place encoding and the effect of fornix transection. Psychobiology 26, 190-204.

Skaggs, W.E., and McNaughton, B.L. (1993). An information-theoretic approach to deciphering the hippocampal code.

Skaggs, W.E., and McNaughton, B.L. (1998). Spatial firing properties of

hippocampal CA1 populations in an environment containing two visually identical regions. J Neurosci 18, 8455-8466.

Skaggs, W.E., McNaughton, B.L., Wilson, M.A., and Barnes, C.A. (1996). Theta phase precession in hippocampal neuronal populations and the compression of temporal sequences. Hippocampus 6, 149-172.

Spence, K.W. (1934). Visual acuity and its relation to brightness in chimpanzee and man. J Comp Psychol 18, 333-361.

Sunyer, B., Patil, S.S., Höger, H., and Lubec, G. (2007). Barnes maze, a useful task to assess spatial reference memory in the mice. Nature Protocols.

Suzuki, S., Augerinos, G., and Black, A.H. (1980). Stimulus control of spatial behavior on the eight-arm maze in rats. Learning and Motivation 11, 1-18.

Tanila, H., Shapiro, M., Gallagher, M., and Eichenbaum, H. (1997). Brain aging: changes in the nature of information coding by the hippocampus. J Neurosci 17, 5155-5166.

Thompson, L.T., and Best, P.J. (1989). Place cells and silent cells in the hippocampus of freely-behaving rats. J Neurosci 9, 2382-2390.

Thompson, L.T., and Best, P.J. (1990). Long-term stability of the place-field activity of single units recorded from the dorsal hippocampus of freely behaving rats. Brain Res 509, 299-308.

Tolman, E.C. (1939). Prediction of vicarious trial and error by means of the schematic sowbug. Psychol Rev 46, 318-336.

Tolman, E.C., and Minium, E. (1942). VTE in rats: overlearning and difficulty of discrimination. J Comp Psychol 34, 301-306.

Tolman, E.C., Ritchie, B.F., and Kalish, D. (1946). Studies in spatial learning. II. Place learning versus response learning. Journal of Experimental Psychology 36, 221-229.

Tolman, E.C., Ritchie, B.F., and Kalish, D. (1947). Studies in spatial learning. IV. The transfer of place learning to other starting paths. Journal of Experimental Psychology 37, 39-47.

Treves, A., and Rolls, E.T. (1992). Computational constraints suggest the need for two distinct input systems to the hippocampal CA3 network. Hippocampus 2, 189-199.

Treves, A., and Rolls, E.T. (1994). Computational analysis of the role of the hippocampus in memory. Hippocampus 4, 374-391.

Vazdarjanova, A., and Guzowski, J.F. (2004). Differences in hippocampal neuronal population responses to modifications of an environmental context: evidence for distinct, yet complementary, functions of CA3 and CA1 ensembles. J Neurosci 24, 6489-6496.

Vincent, S.B. (1915). The white rat and the maze problem: The introduction of a visual control. Journal of Animal Behavior 5, 1-24.

Vinogradova, O.S. (2001). Hippocampus as comparator: Role of the two input and two output systems of the hippocampus in selection and registration of information. Hippocampus 11, 578-598.

Walthall Jr, W.J. (1948). The influence of different maze surroundings on

learning. Journal of Comparative and Physiological Psychology 41, 438-449.

Wang, Z., Bovik, A.C., Sheikh, H.R., and Simoncelli, E.P. (2004). Image quality assessment: from error visibility to structural similarity. IEEE Trans Image Process 13, 600-612.

Wiener, S.I., Korshunov, V.A., Garcia, R., and Berthoz, A. (1995). Inertial, Substratal and Landmark Cue Control of Hippocampal CA1 Place Cell Activity. European Journal of Neuroscience 7, 2206-2219.

Wills, T.J., Lever, C., Cacucci, F., Burgess, N., and O'Keefe, J. (2005). Attractor dynamics in the hippocampal representation of the local environment. Science 308, 873-876.

Wilson, M.A., and McNaughton, B.L. (1993). Dynamics of the hippocampal ensemble code for space. Science 261, 1055-1058.

Wirth, S., Baraduc, P., Plante, A., Pinede, S., and Duhamel, J.R. (2017). Gaze-informed, task-situated representation of space in primate hippocampus during virtual navigation. PLoS Biol 15, e2001045.

Witter, M.P., Wouterlood, F.G., Naber, P.A., and Van Haeften, T. (2000). Anatomical organization of the parahippocampal-hippocampal network. Ann N Y Acad Sci 911, 1-24.

Yang, C.R., and Mogenson, G.J. (1987). Hippocampal signal transmission to the pedunculopontine nucleus and its regulation by dopamine D2 receptors in the nucleus accumbens: an electrophysiological and behavioural study. Neuroscience 23, 1041-1055.

Yoo, S.-W., and Lee, I. (2017). Functional double dissociation within the entorhinal cortex for visual scene-dependent choice behavior. eLife 6, e21543.

Youngstrom, I.A., and Strowbridge, B.W. (2012). Visual landmarks facilitate rodent spatial navigation in virtual reality environments. Learn Mem 19, 84-90.

Yu, Y., Hira, R., Stirman, J.N., Yu, W., Smith, I.T., and Smith, S.L. (2018). Mice use robust and common strategies to discriminate natural scenes. Sci Rep 8, 1379.

Zorzo, C., Arias, J.L., and Mendez, M. (2021). Hippocampus and cortex are involved in the retrieval of a spatial memory under full and partial cue availability. Behav Brain Res 405, 113204.

Zutshi, I., Valero, M., Fernandez-Ruiz, A., and Buzsaki, G. (2022). Extrinsic control and intrinsic computation in the hippocampal CA1 circuit. Neuron 110, 658-673 e655.

Acknowledgement (감사의 말)

긴 시간 동안 저를 인내와 열정으로 지도해주신 이인아 교수님께 진심을 담아 감사의 말씀을 드리고 싶습니다. 특히 박사과정 동안 결혼, 두 아이의 탄생, 육아로 인해 연구실에서 떠나서 있었던 기간이 꽤 길었는데, 저에게 조급해하지 말고 최선을 다하고 돌아오라고 응원해주신 교수님께 감사드립니다. 또한 가상현실 시스템 구축에 큰 도움을 준 승우와 2016년 6월~8월 사이에 인턴으로 지내며 시스템 구축에 앞장서 기여를 한 루니에게도 깊은 감사를 드립니다. Lee lab 연구실 구성원들, 그리고 저와 함께 긴 시간 동안 연구실에서 대부분의 순간과 희로애락을 함께하며 이 논문을 작성한 현우에게 항상 고맙다는 이야기를 남기고자 합니다.

무엇보다도 이 모든 과정을 옆에서 무한한 사랑과 관심으로 응원해주신 할머니, 아빠, 엄마, 장인어른, 장모님께 진심 어린 감사의 말씀을 드리고 싶습니다. 한결같은 마음으로 응원을 해주고 두 아이를 사랑으로 양육하며 본인의 박사학위까지 받아낸 자랑스러운 선영이, 내 성격까지 닮아 조용할 날 없지만 건강하고 무탈하게 잘 커 줘서 예쁜 제인과 예나, 힘들 때마다 탈출구가 되어줬던 빵밴드, 고등학교 시절부터 모든 상황을 진심으로 함께 고민해왔던 정욱이, 10~20대의 청춘을 함께 열정적으로 불태운 성현이, 그리고 평생 연구 동료이자 친구인 현우야 고맙다!

국문초록

해마 하위 영역 CA1과 CA3의 시각 자극 변화에 따른 장소 표상 패턴 연구

신요섭

우리가 일상에서 경험하는 사건들은 하나의 스토리로 구성되어 일화 기억으로 형성된다. 해마는 과거에 경험한 일 들 뿐만 아니라 현재 경험하고 있는 사건들에 대한 일화 기억을 처리할 때 필수적인 뇌 영역이라고 알려져 있다. 설치류의 해마에서 관찰되는 장소 세포는 해마가 동물이 인지하고 있는 공간에 대한 지도를 형성하는 핵심적인 역할을 하는 것으로 알려져 있다. 특히 특정한 공간에서만 선별적으로 발화하는 장소 세포는 환경에 변화가 주어졌을 때 “remapping”이라는 현상으로 환경의 변화를 반영한다고 알려져 있다. 환경에 변화가 있을 때, 장소 세포가 동일한 위치에서 활동하며 발화 빈도를 조정하거나 전혀 다른 장소에서 활동하는 패턴으로 관찰된다. 이러한 장소 세포의 변화는 i) 기존의 기억을 조금 변형하거나, ii) 새로운 기억을 형성하는 일화 기억의 형태를 가지고 있다. 하지만 장소 세포가 불규칙적인 패턴으로 공간의 변화를 표상함에 따라 이들의 활동이 갖는 의미는 불분명하게 남아있다. 또한 장소 세포가 복합적인 감각 정보들을 반영한다는 특징은, 이들이 어떤 인지적 의미를 가지며 활동을 하는 것인지에 대한 난제를 남겼다. 본인은 해마의 장소 세포가 일화 기억에 어떤 기여를 할 것인지, 특히 변화된 환경에서 무엇을 새로 기억하고

기존에 알고 있는 정보는 어떻게 처리할 것인지 연산하는 과정을 해마의 하위 영역인 CA1과 CA3에서 각각 어떻게 표상하는지 알아보고자 하였다. 이에 대한 답을 찾기 위해 본인은 동물이 상호작용하며 경험할 수 있는 가상 현실 (VR) 시스템을 제작하여 가상 환경의 시각 자극을 정량적으로 조작하였다. 이 과정에서 본인은 동물이 경험하는 시각 자극의 변화와 (i.e., input) 해마 장소세포의 전기적 활동 (i.e., output) 간의 관계를 조사하였다. 첫 번째 질문으로는 본인이 구축한 가상 현실 시스템에서 장소 세포가 발현되는지를 확인하였다. 그 결과로 기존 문헌에서 보고되었던 결과와 비슷한 수준의 장소 세포들을 검증할 수 있었다. 본인이 구축한 가상 현실 시스템에서 장소 세포가 관찰된다는 것을 확인한 이후에는, 기존 환경에 정량적인 시각적 변화를 주어 장소 세포가 해당 변화를 어떻게 반영하는지 질문하였다. 그 결과로, 해마의 하위 영역 CA1에서 기존 환경에 대한 표상을 유지하는 집단과, 특정 환경에 변화가 가해진 사건에 의해 새로운 표상을 유지하는 집단이 동시다발적으로 나뉜다는 현상을 관찰하였다. 반면, 해마 하위 영역인 CA3에서는 환경에 변화가 이루어졌음에도 불구하고 대부분의 장소 세포들이 기존 환경에 대한 표상을 유지하였다. 이러한 결과를 토대로 해마 하위 영역인 CA3은 기존에 알고 있던 환경에 대한 기억을 안정적으로 유지하는 역할을 수행하는 반면, 해마 하위 영역인 CA1은 변화하는 환경 내에서도 이전의 기억과 새로운 기억을 독립적으로 구분하여 새로운 정보를 유연하게 학습하도록 하는 가능성을 제시하고자 한다.